AMES FILE
COPY No. 1

NASA

TECHNICAL MEMORANDUM
X-94

EFFECTS OF UNSYMMETRICAL AIR-FLOW CHARACTERISTICS OF

TWIN-INTAKE AIR-INDUCTION SYSTEMS ON AIRPLANE

STATIC STABILITY AT SUPERSONIC SPEEDS

By Warren E. Anderson and Edward W. Perkins

Ames Research Center
Moffett Field, Calif.

CLASSIFIED DOCUMENT - TITLE UNCLASSIFIED

NATIONAL AERONAUTICS AND SPACE ADMINISTRATION

WASHINGTON   December 1959

NATIONAL AERONAUTICS AND SPACE ADMINISTRATION

TECHNICAL MEMORANDUM X-94

EFFECTS OF UNSYMMETRICAL AIR-FLOW CHARACTERISTICS OF

TWIN-INTAKE AIR-INDUCTION SYSTEMS ON AIRPLANE

STATIC STABILITY AT SUPERSONIC SPEEDS[*]

By Warren E. Anderson and Edward W. Perkins

SUMMARY

Twin-duct flow asymmetry and its effect on static stability was investigated on three complete airplane configurations. The test Mach number range extended from 1.6 to 2.35. Reynolds number per foot varied from 2.4×10^6 to 1.7×10^6 for this Mach number range. The angle of attack was varied from -2° to $+15^\circ$ and angle of sideslip from -5° to $+7^\circ$.

The results show that flow asymmetry is promoted at reduced mass-flow ratios. Associated with flow asymmetry are high levels of internal flow unsteadiness; there are also significant variations in fuselage and wing surface pressures which affect the lateral stability.

Previously published flight simulation studies show that the stability increments measured in the wind tunnel account for the oscillations encountered in flight.

Flow deflectors forward of the inlet station were found to reduce flow asymmetry effectively with no adverse effect on airplane static stability.

INTRODUCTION

Twin-intake air-induction systems have been used extensively for jet aircraft operating at subsonic and supersonic speeds. Such a system utilizes symmetrical twin intakes which join in a common duct at a station forward of the engine compressor. Although this type of system can give relatively high efficiency, it is susceptible to twin-duct flow

---

[*]Title, Unclassified

instability characterized by inlet flow asymmetry when operated at reduced mass-flow conditions. The inherent flow asymmetry of twin-inlet systems has been analyzed in references 1 and 2 and found to be associated with the static-pressure characteristics of the individual ducts.

Wind-tunnel observations of twin-duct flow asymmetry at supersonic speeds have been reported in references 3, 4, and 5. Reference 3 also indicates that flow unsteadiness or "buzz" can occur simultaneously with flow asymmetry. Flight experience such as that reported in reference 6 indicates duct-flow asymmetry produces an unbalance of pressure forces on the airplane which leads to severe aircraft stability and control problems. Heretofore, wind-tunnel measurements of these forces, knowledge of which are necessary to any analysis of the stability variations involved, have not been reported.

The purpose of this investigation was to examine the nature of asymmetrical flow in twin-intake systems at supersonic speeds and to measure the effects on airplane static stability. These measurements were then utilized together with flight simulation techniques to explain the adverse effects of flow asymmetry on aircraft dynamics as recorded in flight. Possible methods of alleviating the unfavorable stability characteristics were also investigated.

Force and pressure measurements were obtained for each of three complete twin-duct airplane configurations. One model (Model A) was investigated more extensively than the other two. For this model the test Mach numbers were 1.6, 1.8, 2.0, and 2.35. The Reynolds number per foot varied from 2.4×10^6 to 1.7×10^6 for this Mach number range. The angle of attack was varied from $-2°$ to $+15°$ and angle of sideslip from $-5°$ to $+7°$. Models B and C were investigated for slightly different values of α and β at Mach numbers of 2.2 and 2.1, respectively.

SYMBOLS

A duct cross-section area, sq ft

A_c duct capture reference area, sq ft

b wing span, ft

c wing chord, ft

C_l rolling-moment coefficient, stability axis, $\dfrac{l}{qSb}$

C_n yawing-moment coefficient, stability axis, $\dfrac{n}{qSb}$

d   distance from reference station, in.

l rolling moment, ft-lb

$\dfrac{m_3}{m_\infty}$ inlet mass-flow ratio, $\dfrac{\rho_3 V_3 A_3}{\rho_\infty V_\infty A_C}$

M   Mach number

MAC   mean aerodynamic chord, ft

n   yawing moment, ft-lb

p   pressure, lb/sq ft

P   pressure coefficient, $\dfrac{p_l - p_\infty}{q_\infty}$

Δp peak to peak static-pressure fluctuation, lb/sq ft

q   dynamic pressure, lb/sq ft

S   wing area, sq ft

V   velocity, ft/sec

α angle of attack, deg

β angle of sideslip, deg

ρ mass density, slugs/cu ft

Subscripts

l local

t   total stagnation

∞ free stream

3   compressor rake

CONFIDENTIAL

TEST APPARATUS

Models

Three complete airplane configurations were tested in the 9- by 7-foot test section of the Ames Unitary Plan wind tunnel. Photographs of these models mounted in the wind tunnel are shown in figures 1(a), 2(a), and 3(a). Drawings showing pertinent model dimensions are presented in figures 1(b), 2(b), and 3(b), and general inlet details for each model are shown in figures 1(c), 2(c), and 3(c). Each model incorporated a twin-intake air-induction system. Model A included a half-conical side-scoop system while Models B and C employed a double-ramp top-scoop and a double-ramp side-scoop system, respectively.

Fuselage boundary-layer diverters were utilized for all three duct configurations. For Model A the diverter was formed by undercutting the fuselage-mounted cone a varying height from the apex to the cowl lip station. Also, the inner cowl lip was displaced from the fuselage surface to prevent external boundary-layer air from entering the inlet. Inlets for Models B and C were displaced outward from the fuselage surface so as to make space available to form the diverters. A portion of the fuselage boundary-layer flow of Model C was taken internally (see fig. 3(c)). Model B incorporated internal duct bleed on the compression surfaces, shown in figure 2(c), which was approximately 10 percent of the main duct flow.

Instrumentation

Static forces were measured for all models with a six-component strain-gage-type sting balance and were recorded by a balanced-bridge automatic readout system. Model A was also instrumented with resistance-type pressure transducers for instantaneous measurement of total- and static-pressure fluctuations within each of the two ducts. Balance and transducer measurements were recorded on a multichannel light-beam oscillograph.

Total- and static-pressure measurements were made with multitube rakes located at the simulated compressor face. Over-all pressure ratios as presented are area-weighted averages of the individual tube values. External static-pressure measurements were obtained with flush orifices on the fuselage surface. All pressure measurements were recorded photographically from back-lighted, multiple-tube, mercury manometers.

Translating plugs mounted at the exits of the internal ducts controlled the mass flow for Models A and C. Model B made use of an iris

CONFIDENTIAL

diaphragm for this purpose. The plug controlled exit areas were cali-
brated for choked flow conditions to permit computation of mass-flow
ratio. For model B a venturi meter was used for mass-flow measurement.

Visual studies of the external flow were made with a single pass
schlieren system with facilities for obtaining photographs and motion
pictures of the flow fluctuations.

TEST PROCEDURE

The basic longitudinal and lateral stability characteristics of
each model were established for a range of angles of attack and sideslip
with the twin-inlet system operating at maximum mass-flow conditions.
For each angle of attack the models were then positioned for an angle of
sideslip of 0° and the duct mass-flow ratio was reduced until visual
indications of flow asymmetry were observed. Force and pressure measure-
ments were then obtained for the same schedule of angles of sideslip used
in establishing the basic stability characteristics. No attempt was made
to maintain constant duct mass-flow ratio as the model attitude departed
from the zero sideslip condition. Model A was tested at two conditions
of reduced mass flow, representing both slight and relatively severe
inlet flow asymmetry. Also, the flow in one of the ducts of Model A was
completely blocked to determine maximum flow asymmetry effects. Force
measurements at only one reduced mass flow representing severe inlet
flow asymmetry were made for Models B and C.

The foregoing procedure was also followed for each model with the
tail removed to determine the interaction between the inlet flow asymmetry
and the tail surfaces.

Flow spoilers were mounted on the half-cone center bodies of Model A
in an attempt to eliminate flow asymmetry. Measurements taken were
similar to those for the basic model but extended to lower mass-flow
ratios which simulated engine windmill air-flow requirements.

RESULTS AND DISCUSSION

Internal Flow Characteristics of Twin-Inlet Systems

Curves showing static- and total-pressure ratios versus mass-flow
ratio are presented in figure 4 for the twin-intake system of Model A.
These curves represent system measurements made at the simulated com-
pressor station in the common duct and no attempt was made to maximize
inlet performance. Although the maximum control-plug flow area did not
permit this system to operate supercritically, data for the unyawed case

show that both static- and total-pressure ratio curves undergo a sharp change in slope at a reduced value of mass-flow ratio. This change in slope is accompanied by twin-duct flow asymmetry. Schlieren photographs showing shock wave patterns for representative data points noted D and E in figure 4 are presented in figure 5.

The phenomenon of flow asymmetry in twin-intake systems has been analyzed in references 1 and 2. It was shown that the basic requirements of flow continuity relate asymmetry primarily to individual duct static-pressure characteristics. For the requirement of a uniform static pressure across the entrance to the common duct a positive slope (decreasing static pressure with decreasing mass-flow ratio) is the basis of instability since it does not readily permit equal flow in both ducts; rather, the flow quantities in the individual ducts diverge as system mass flow is reduced until reversed flow is experienced in one of the ducts.

Under flow conditions at $\beta = 0^{\circ}$ the system characteristics shown in figure 4 are typical and the simplified sketch below relates these characteristics to those of the individual ducts. System performance is identical to that of the individual ducts at high mass-flow ratios since the
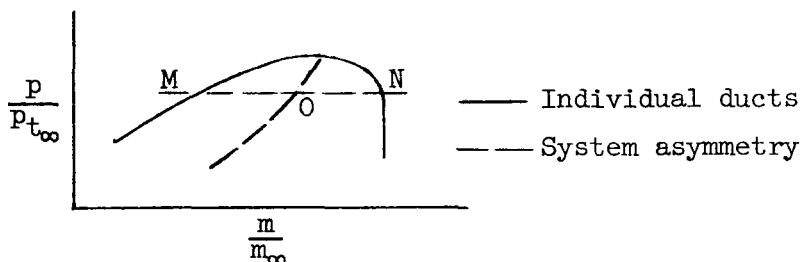
static-pressure variation with mass flow allows symmetrical twin-inlet operation. In the range of mass-flow ratios less than that for maximum static-pressure ratio, however, the two inlets operate asymmetrically, for example at points M and N in the sketch. Flow continuity requirements result in corresponding system performance at point O and generally in a rapid drop in system static pressure with decreasing mass-flow ratio.

For $\beta = \pm 3^{\circ}$, figure 4, the slope of the system static-pressure ratio curve was positive throughout the entire range of mass-flow ratio measured and flow asymmetry was always present with no apparent stable range of mass flow. References 4 and 5 indicate that a reduction in the symmetric or stable mass-flow range with increasing angles of sideslip can be expected.

Static-pressure unsteadiness for the individual ducts of Model A is presented in figure 6. Again the Mach number considered is 2.0. For 0° sideslip the unsteadiness of both ducts increased sharply as the mass-

flow ratio was reduced below point D to the value at which flow asymmetry was observed (point E, see also figs. 4 and 5). Schlieren observations at angles of sideslip near zero, however, indicated a random, high-frequency switching of the subcritical and supercritical flow conditions between the two inlets. Pressure fluctuations imposed by this switching phenomenon dominated the frequency-amplitude spectrum and, as a result, both inlets exhibited similar levels of unsteadiness.

When the angle of sideslip was increased to 3° the left or leeward duct flow was always subcritical and, as shown, the unsteadiness was considerably greater than for the right or windward duct which experienced supercritical flow throughout the mass-flow range. The unsteadiness or buzz associated with reduced flow in the leeward duct under conditions of flow asymmetry was undoubtedly due to shock-wave boundary-layer inter-action forward of the conical center body. The "slip line" phenomenon explained in reference 7 could also have contributed to the unsteadiness. The magnitude of pressure fluctuation was substantially reduced at low values of mass-flow ratio reflecting the small quantity of flow being handled by the leeward duct. Flow reversal in this duct is possible under these conditions.

The effect of flow asymmetry on fuselage static-pressure distributions near the inlet is shown in figure 7. The flow asymmetry associated with minimum subcritical flow was simulated by completely plugging one duct which was instrumented with flush pressure orifices as shown in the sketch. The results show that large positive pressures appear on the fuselage forward of an inlet during reduced flow operation. The resulting force acts substantially ahead of the center of gravity. Supercriti-cal flow which occurs simultaneously through the opposite duct is shown to maintain higher pressures aft of the inlet than those of similar location on the subcritical side. Although the two forces tend to oppose each other, it seems clear that because of its longer moment arm, the forward force predominates and subcritical flow in a leeward duct has a net effect of increasing the yawing or restoring moment on the fuselage.

In summary, twin-inlet systems are fundamentally susceptible to flow asymmetry at reduced values of mass flow. The flow asymmetry has pronounced effect on the fuselage static-pressure distribution. In addition, for sideslip angles between approximately $\pm 2^\circ$, flow asymmetry is unsteady and flow conditions in the ducts reverse in random fashion.

Effects of Flow Asymmetry on Static Stability

Model A.- Yawing-moment and rolling-moment coefficients with corre-sponding mass-flow ratios are plotted as a function of the angle of

sideslip in figure 8 for a Mach number of 2.0. Data are presented for full-flow and reduced-flow control-plug settings. The full-flow setting with one duct completely plugged is also shown.

In figure 8(a) for an angle of attack of 1.0^O the directional stability, C_{n_β}, was normal and sensibly linear for full-flow duct conditions. A reduction in mass-flow ratio of about 50 percent resulted in discontinuous yawing-moment variations near zero sideslip and an increase in C_n by 0.002 to 0.003 at angles of sideslip greater than $\pm 2^O$. Observations at these higher angles showed that subcritical flow existed in the leeward duct and supercritical flow in the windward duct similar to that illustrated in figure 5. A somewhat greater increase in C_n was obtained by plugging the left duct even though the system mass-flow ratio was greater than that for the reduced flow setting. At this setting the lower mass-flow values evidently resulted from reversed flow occurring in the leeward duct.

The effects of twin-duct instability or switching are evident in the range $-2^O \lessgtr \beta \lessgtr +2^O$; the incremental changes in C_n were the same as at higher angles of sideslip. The instability was triggered by unsteady flow associated with the subcritical duct during asymmetric operation. It appears that even though there was considerable unsteadiness in the range of sideslip angles greater than about $\pm 2.0^O$ the stabilizing effect of sideslip prevented switching.

In figure 8(b) the angle of attack has been increased to 8.6^O and a reduction in mass-flow ratio again resulted in subcritical flow in the leeward duct at high angles of sideslip. However, contrary to the results for $\alpha = 1.0^O$ reduced mass flow decreased C_n and increased the rolling-moment coefficient C_l. Balance force measurements and static-pressure distribution studies for $\alpha = 8.6^O$, compared to those for $\alpha = 1.0^O$, indicate a rearward shift in the center of pressure on the fuselage due to the subcritical duct flow field. The result is a reduction in C_n. Also, the flow field reduces the lift of the leeward wing, thus increasing C_l.

Longitudinal stability was found to be unaffected by duct flow asymmetry over the range of α and β tested.

The tail-off lateral characteristics of Model A are presented in figure 9. Comparison of figures 9(a) and 8(a) shows the same incremental effects due to mass-flow ratio, indicating the tail was unaffected by duct flow asymmetry at $\alpha = 1.0^O$. For the high-angle-of-attack case shown in figure 9(b), the yawing-moment curve for reduced flow is displaced below the full-flow curve. The reason for this is not clear; however, the change in lateral stability due to mass-flow ratio is in the same direction and of the same general increment as for the tail-on

case of figure $8(b)$. Again, the tail effect would seem to be minor, indicating the fuselage pressures to be mainly responsible for reduced values of C_n at angle of attack.

In summary, flow asymmetry, occurring as a result of reduced inlet flow, caused substantial changes in airframe static lateral stability. The effects which varied somewhat with angle of attack were primarily a result of changes in the fuselage pressures, inasmuch as adding or removing the tail surfaces had no significant effect on the incremental changes in the lateral stability parameters.

Models B and C.- The inlet systems for Models B and C were both located above the wing. This was in contrast to that of Model A which had a mid-wing location. A comparison of figures 10(a) and 11(a) with figure 8(a) shows the change in lateral stability characteristics with reduced inlet flow at low angles of attack to be similar for all three configurations. Increasing the angle of attack to approximately 7° (figs. 10(b) and 11(b)) did not, however, reverse the effects of low mass flow as in the case of Model A. Thus, it appears that the interference effects of duct flow asymmetry on airplane lateral stability depend on the inlet location with respect to both fuselage and wing. Further investigation of this effect would seem desirable. Twin-duct instability is not indicated by the data points of figures 10 and 11 but flow observations during the test substantiated its existence at low angles of yaw (dashed curves) similar to Model A.

It should be stated that the inlets of Models B and C incorporate the idea of a variable second ramp. Proper scheduling of the second ramp angle gives these systems the capability of greatly reducing the adverse effects of flow asymmetry.

Tail-off tests for these models again showed the effect of flow asymmetry on tail loads to be negligible. Stability characteristics for Model B were obtained from reference 8.

Wind Tunnel Data Applied to Flight Performance - Model A

The incremental changes in yawing- and rolling-moment coefficients caused by twin-inlet flow asymmetry at reduced mass-flow ratio are shown in figure 12 for the test Mach number range. The data suggest that two operating modes could exist in flight at these Mach numbers as illustrated in figure 13. The first flight mode would occur at low-angle-of-attack conditions and could support a yawing oscillation as follows: An initial disturbance resulting in flow asymmetry would increase the yawing moment and establish a yawing rotation which would tend to trim the aircraft at a small angle of yaw. However, the rotation would necessarily be in a direction causing reversal of flow asymmetry which would, in turn, change

direction of the yawing motion. Repetition of this cycle could be expected to increase the amplitude of the oscillation, making the aircraft dynamically unstable in yaw.

The other flight mode would occur at high-angle-of-attack attitudes and would not be subject to oscillation. Flow asymmetry would result in a direction of rotation which would resist reversal of duct flow conditions. As a consequence, the airplane would assume a fixed attitude in yaw at which the incremental yawing moment due to flow asymmetry would be balanced by the moment generated by the vertical stabilizer. At high angles of attack rolling conditions might be manifested as indicated by the data in figure 8(b).

Aircraft flight characteristics can be readily obtained by simulation studies requiring simultaneous solution of the equations of motion involved. If these equations are modified so as to include the disturbances in yaw and roll shown by the wind-tunnel data of figure 12, and in the manner shown in figure 13, aircraft flight motions can be studied on a time-history basis.

The results of a simulation study are reported in reference 9 and a comparison of flight measurements and simulator results is reproduced in figure 14 for the low-angle-of-attack mode at an initial Mach number of 2.0. Mach number for the flight measurements decreased to 1.85 as a result of reduced engine thrust and possibly accounts for the phase lag variance indicated. It is evident that the simulator studies give an accurate picture of the flight motions, agreeing well in both amplitude and frequency. Figure 14 shows that the incremental changes in static stability that result from flow asymmetry can be responsible for rather violent dynamic oscillations in flight.

Flow Stabilization of Twin-Inlet Systems

A number of possibilities for reducing the adverse effects of flow asymmetry in twin-inlet systems present themselves. One approach has been to reduce the flow interdependence of the two ducts by eliminating any common ducting. This is done by extending the individual diffusers so that the common duct juncture occurs at the forward face of the engine (see ref. 6).

Another approach incorporates flow stabilizers or deflectors which, when extended, create a symmetrical shock pattern with an attendant decrease in the mass flow in both ducts. Also, the attendant thrust loss and drag rise promote deceleration without requiring a reduction in throttle position. Figure 12 indicates the effects of decreasing speed are favorable to reducing oscillations resulting from asymmetric

duct flow. The performance penalties associated with the use of deflectors preclude their use at conditions other than flame-out or mechanical failure.

A flow stabilizer investigation has been reported in reference 10. Two types of flow deflectors, a cone plug and tilting cone, were found to satisfy requirements for symmetric shock patterns and provided performance within acceptable limits of flow distortion and unsteadiness at the compressor station. The cone plug and tilting cone deflectors are shown mounted on the conical centerbodies of Model A in figure 15. Both configurations were tested and found to give comparable results. A dimensional sketch of the tilting cone deflector is shown in figure 16. Typical results from this arrangement at three Mach numbers are compared to those of the basic model in figure 17. It is seen that with the flow deflectors there is no appreciable change in the basic lateral stability at simulated engine windmill conditions (minimum flow). Schlieren photographs in figure 18 for $M_\infty = 2.0$ show a flow comparison of the basic model with and without deflectors. The schlieren photographs indicate strong shock patterns are associated with the deflectors, however, and a large drag rise can be expected.

CONCLUDING REMARKS

The phenomenon of flow asymmetry in twin-intake air induction systems was investigated on three complete airplane configurations at Mach numbers within the range from 1.6 to 2.35.

During asymmetric flow conditions high levels of unsteadiness were associated with the internal flow of the subcritical duct. Also, reduced duct flow significantly altered the external flow pattern so that the resulting variation in fuselage and wing surface pressures substantially affected the lateral stability.

Previously published flight simulation studies showed that the increments in C_{n_β} and C_{l_β} measured in the wind tunnel account for the oscillations that occur when flow asymmetry is encountered in flight.

Flow deflectors mounted on the conical compression surfaces of the intake were found to be an effective means of reducing flow asymmetry with no adverse effect on airplane static stability.

Ames Research Center
        National Aeronautics and Space Administration
            Moffett Field, Calif., May 22, 1959

REFERENCES

1. Martin, Norman J., and Holzhauser, Curt A.: Analysis of Factors Influencing the Stability Characteristics of Symmetrical Twin-Intake Air-Induction Systems. NACA TN 2049, 1950.

2. Beke, Andrew: Criteria for Initial Flow Reversal in Symmetrical Twin-Intake Air-Induction Systems Operating at Supersonic Speeds. NACA RM E55L02a, 1956.

3. Mossman, Emmet A., Pfyl, Frank A., and Lazzeroni, Frank A.: Experimental Investigation at Mach Numbers From 0 to 1.9 of Trapezoidal and Circular Side Inlets for a Fighter-Type Airplane. NACA RM A55D27, 1955.

4. Obery, Leonard J., Stitt, Leonard E., and Wise, George A.: Evaluation at Supersonic Speeds of Twin-Duct Side-Intake System With Two-Dimensional Double-Shock Inlets. NACA RM E54C08, 1954.

5. Stitt, Leonard E., Cubbison, Robert W., and Flaherty, Richard J.: Performance of Several Half-Conical Side Inlets at Supersonic and Subsonic Speeds. NACA RM E55J10a, 1956.

6. Nugent, Jack: Nonsteady Flow of a Twin-Duct Propulsion System and Airplane Coupling Slightly Below a Mach Number of 2.0. NASA TECH MEMO X-54, 1959.

7. Ferri, Antonio, and Nucci, Louis M.: The Origin of Aerodynamic Instability of Supersonic Inlets at Subcritical Conditions. NACA RM L50K30, 1951.

8. Gnos, Vernon A., and Kurkowski, Richard L.: Static Longitudinal and Lateral Stability and Control Characteristics of a Model of a Swept-Wing Fighter-Bomber-Type Airplane With a Top Inlet at Mach Numbers From 1.6 to 2.35. NACA RM A57K20, 1958.

9. Klampe, D. G., Feistel, T. W., and Celniker, L.: Airplane Dynamic Behavior Resulting From Inlet Duct Flow Instability. Lockheed Rep. 12275, May 15, 1957.

10. Sibley, P. J., and Cambell, D. H.: Induction System Flow Stabilizer Program. Lockheed Rep. 12274, May 15, 1957.
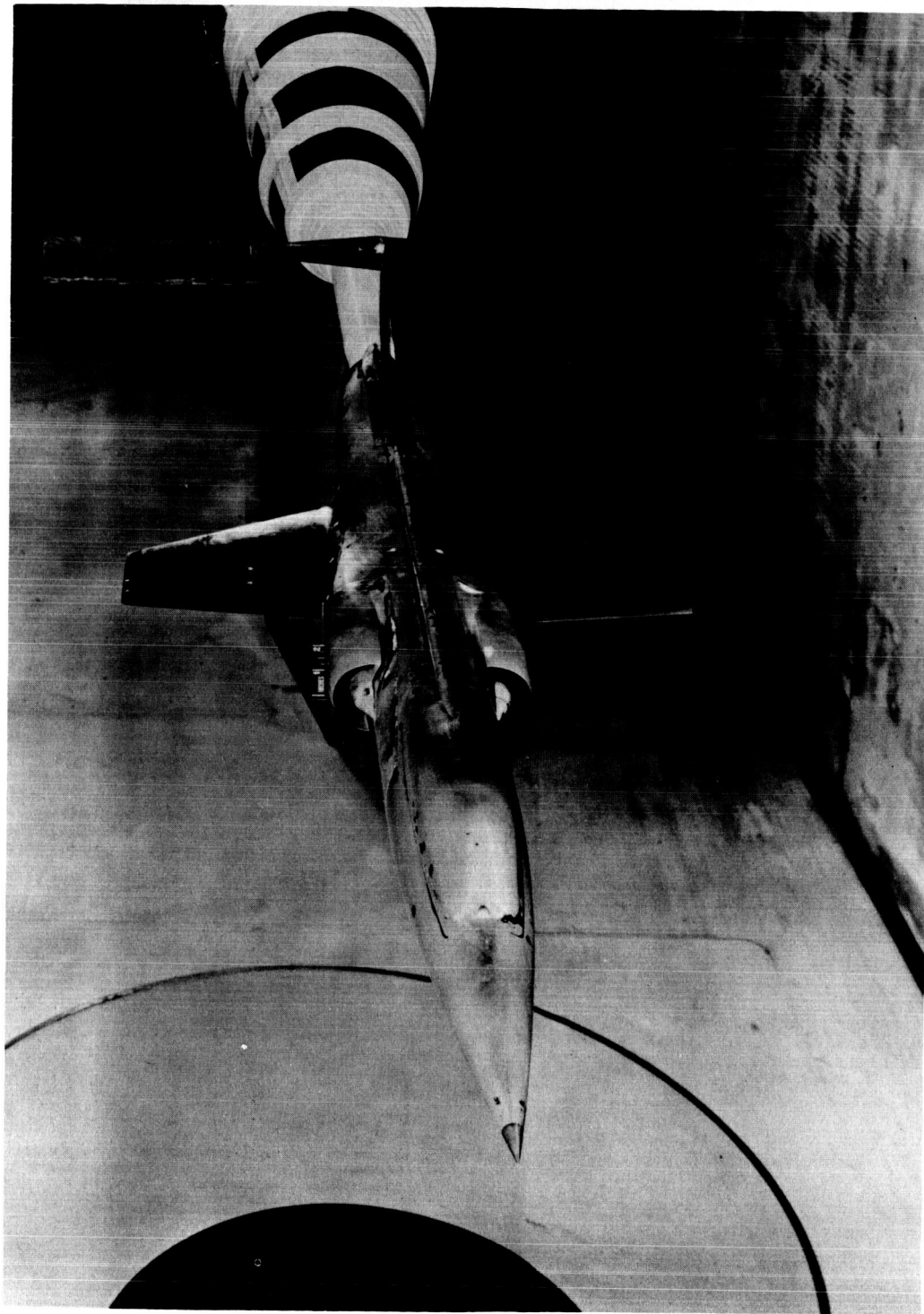
A-23420

(a) Photograph of wind-tunnel installation.

Figure 1.- Photograph and drawings showing details of Model A.
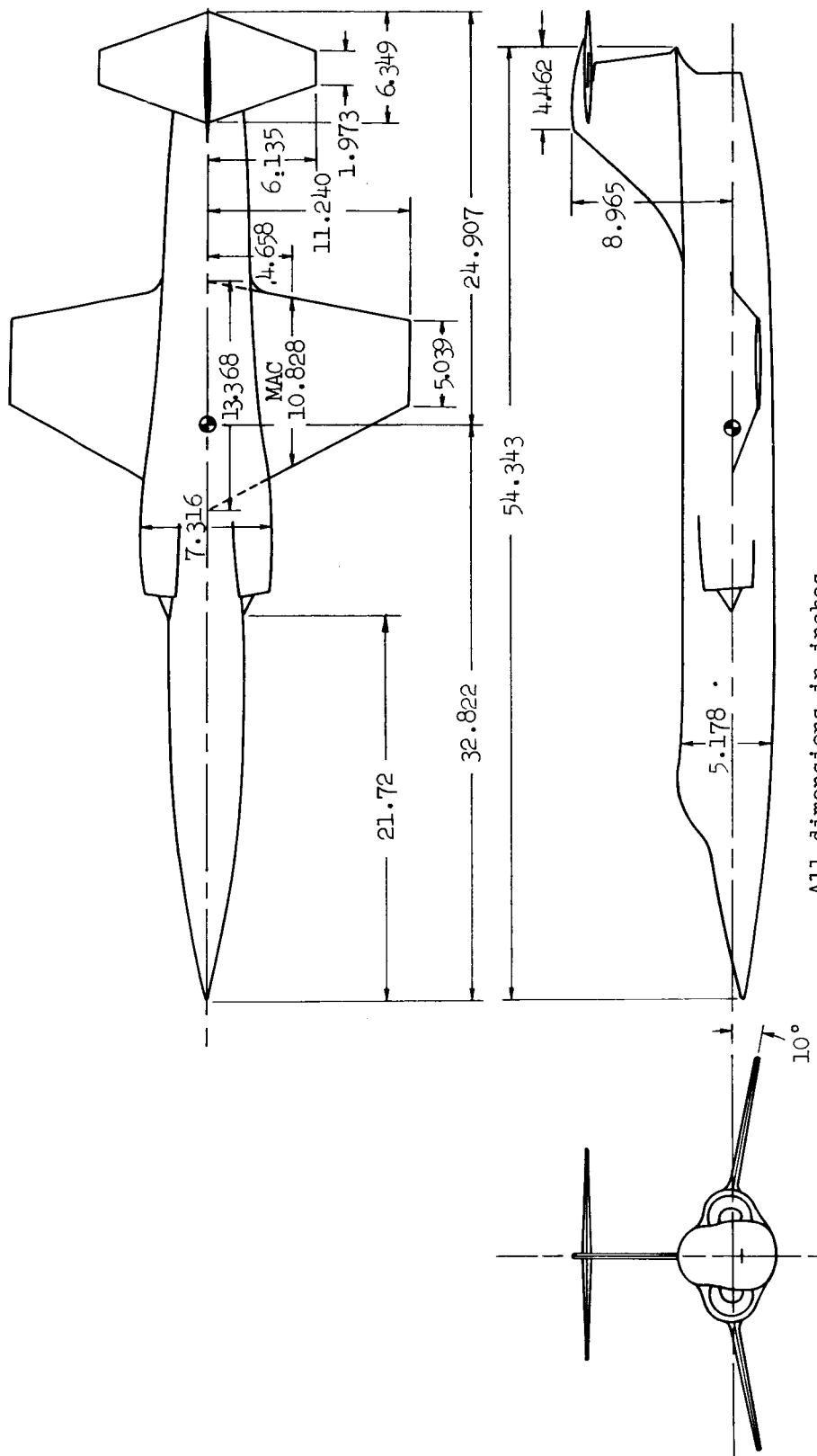
All dimensions in inches.

(b) Three-view drawing.

Figure 1.- Continued.
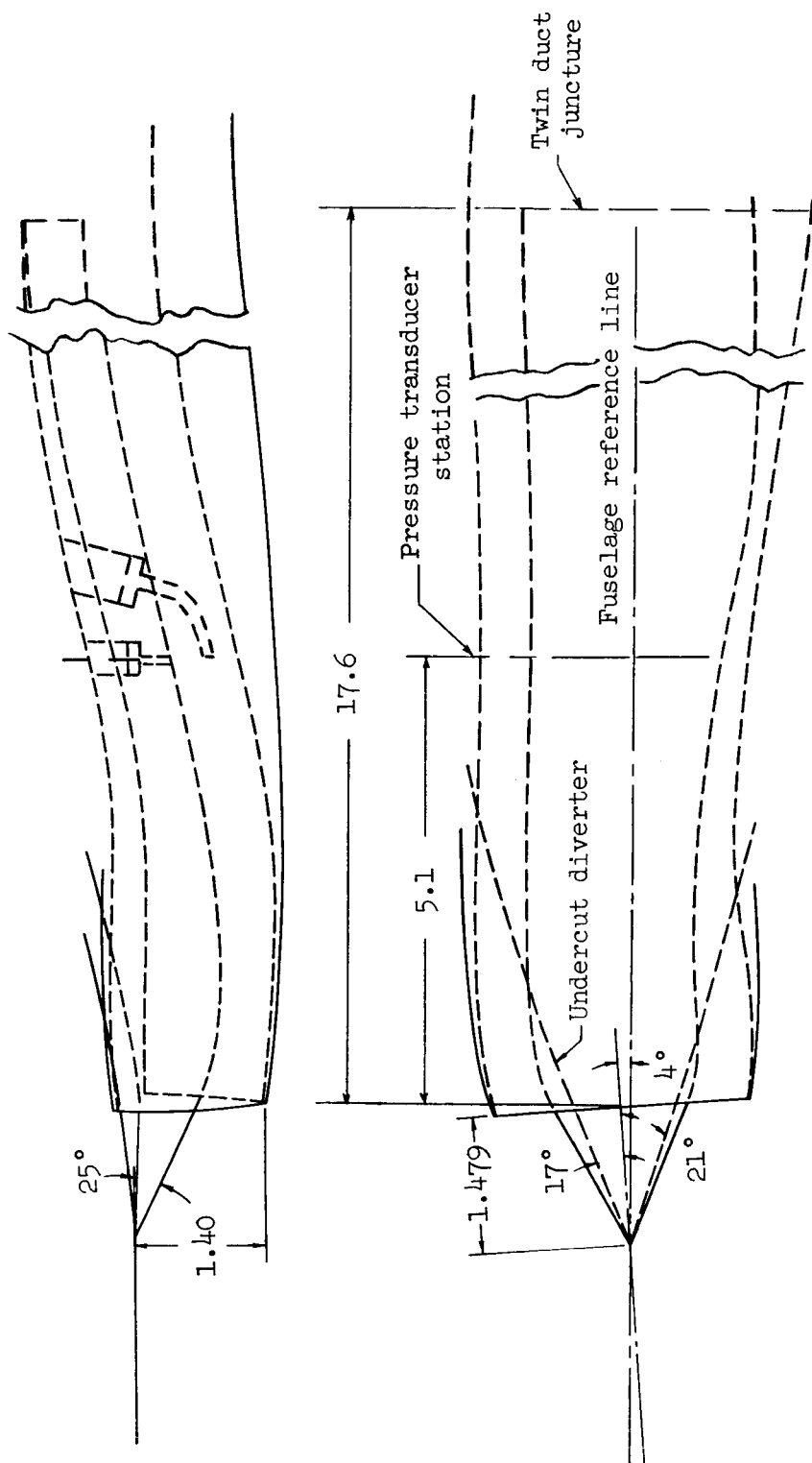
All dimensions in inches.

(c) Inlet details.

Figure 1.- Concluded.
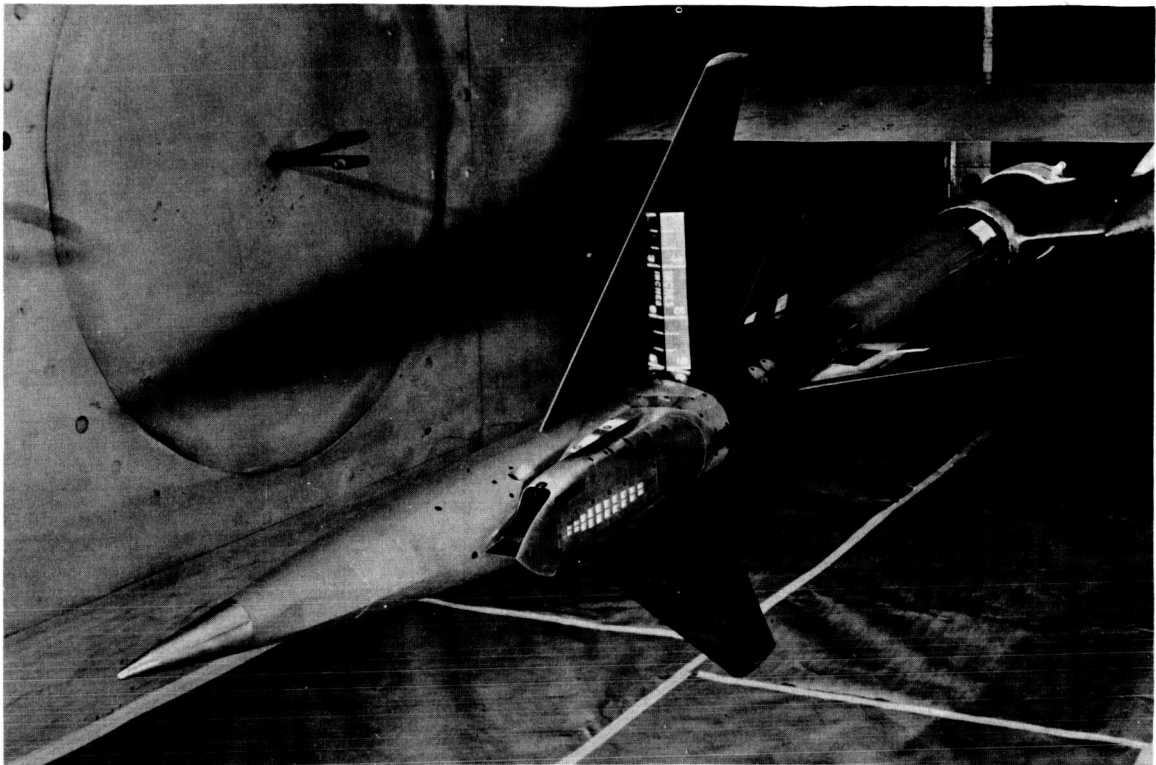
A-21404

(a) Photograph of wind-tunnel installation.

Figure 2.- Photograph and drawings showing details of Model B.
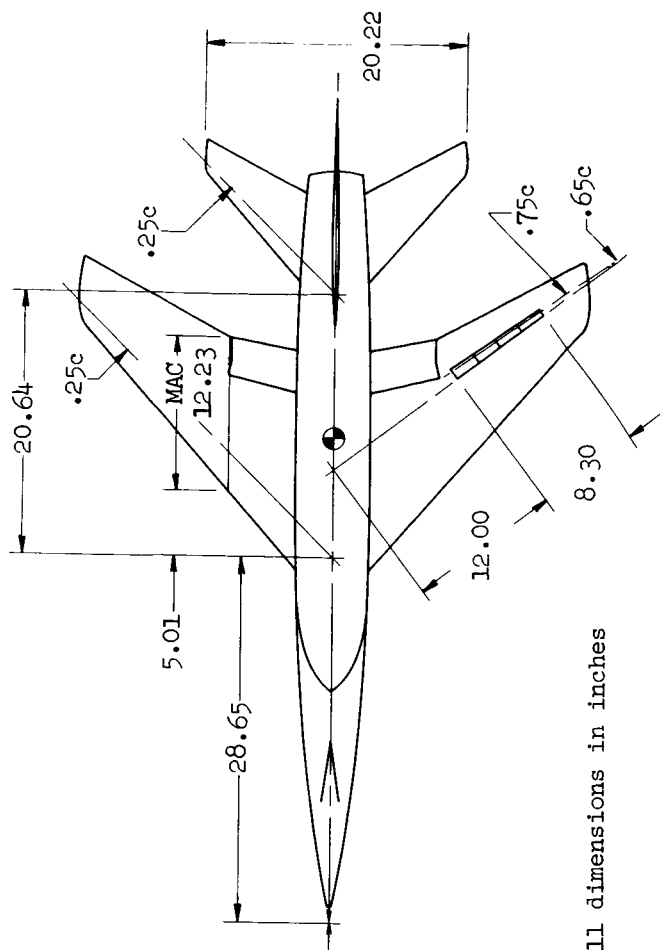
All dimensions in inches
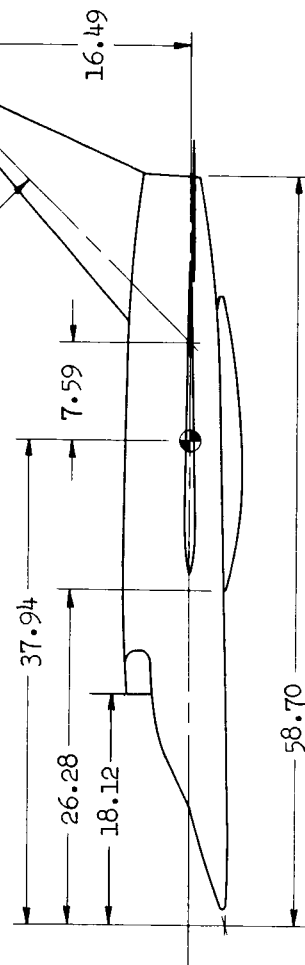
(b) Three-view drawing.

Figure 2.- Continued.

(Second ramp) 19°

(First ramp) 6° Half angle

3.44

Bleed exhaust

Porous bleed plates

1.8

.20
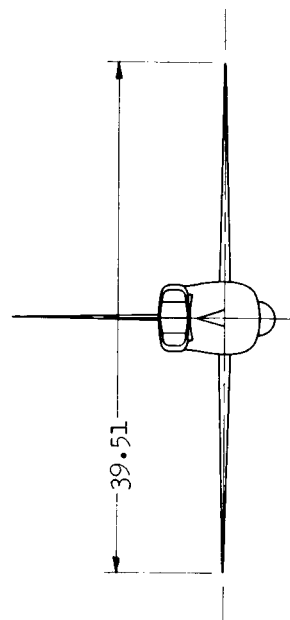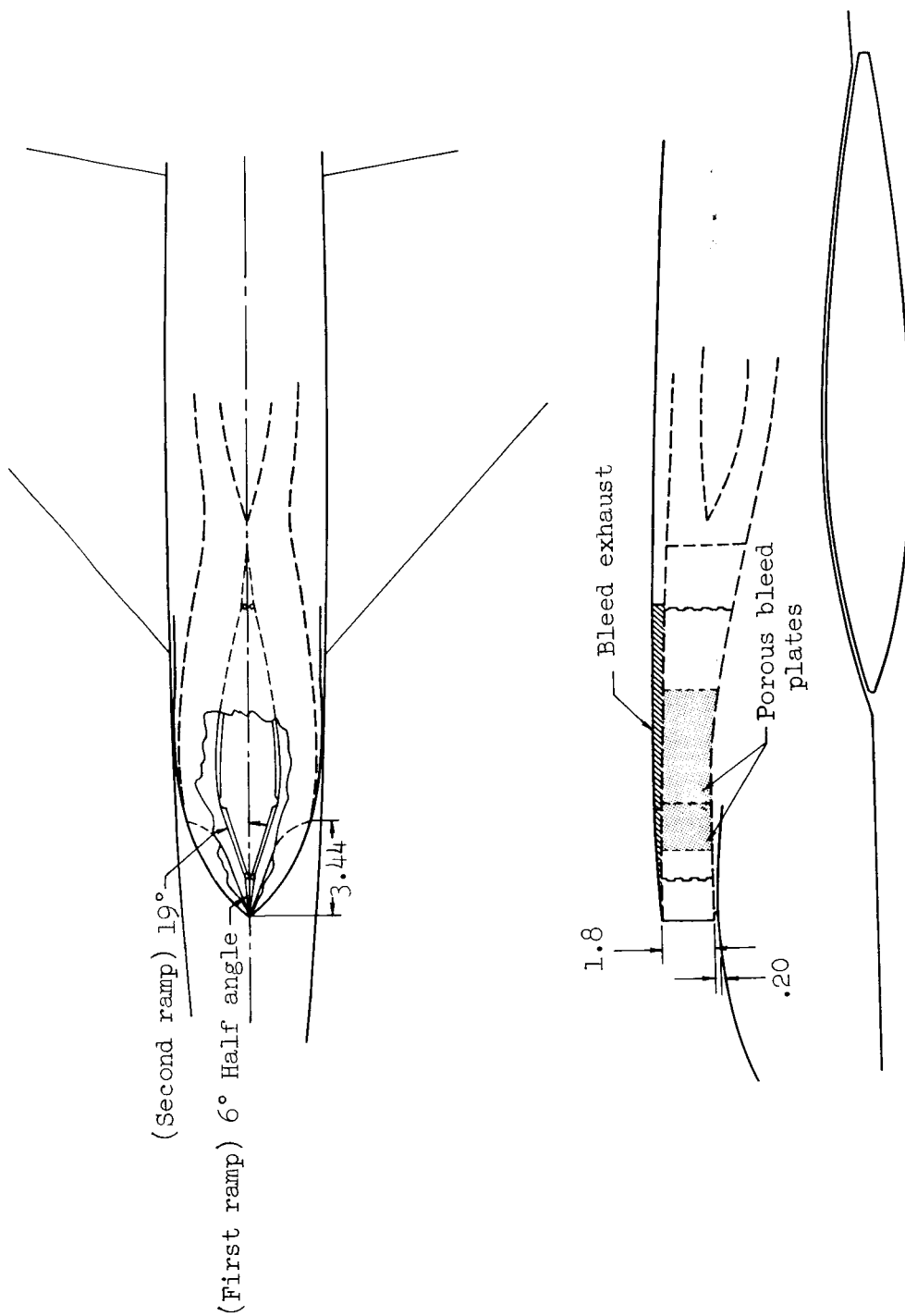
(c) Inlet details.

Figure 2.- Concluded.
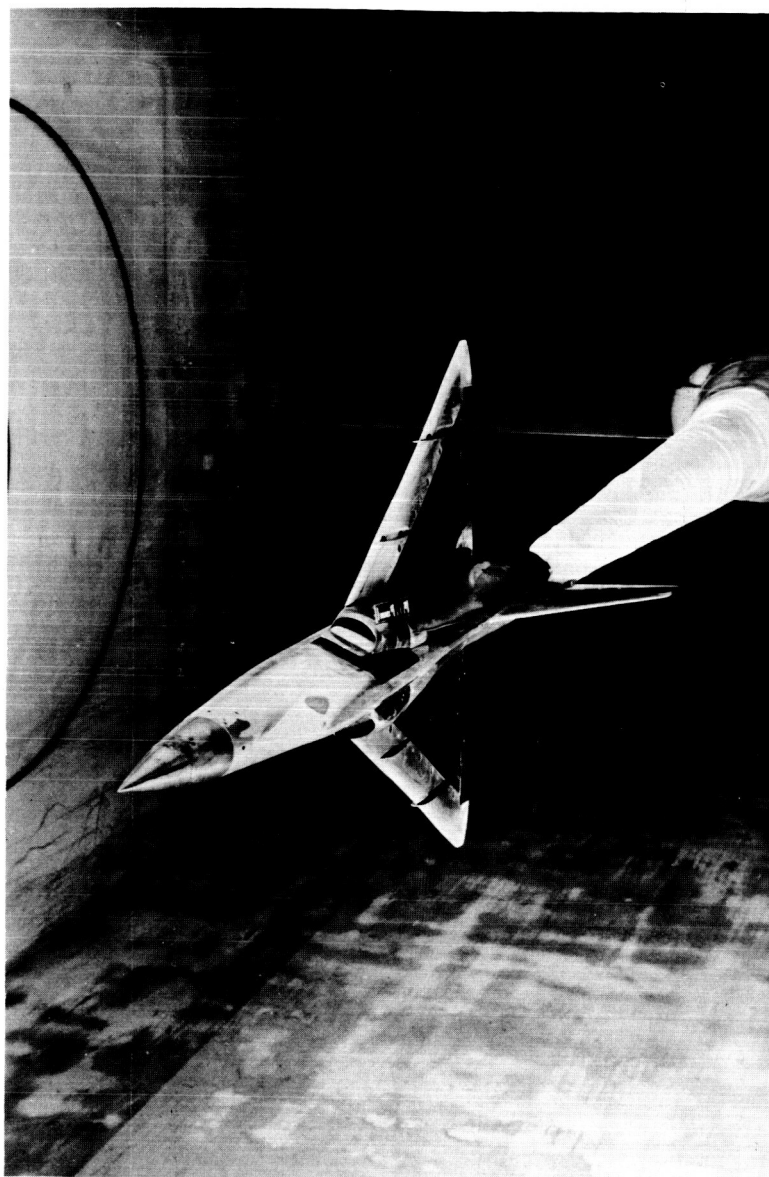
A-23285

(a) Photograph of wind-tunnel installation.

Figure 3.- Photograph and drawings showing details of Model C.
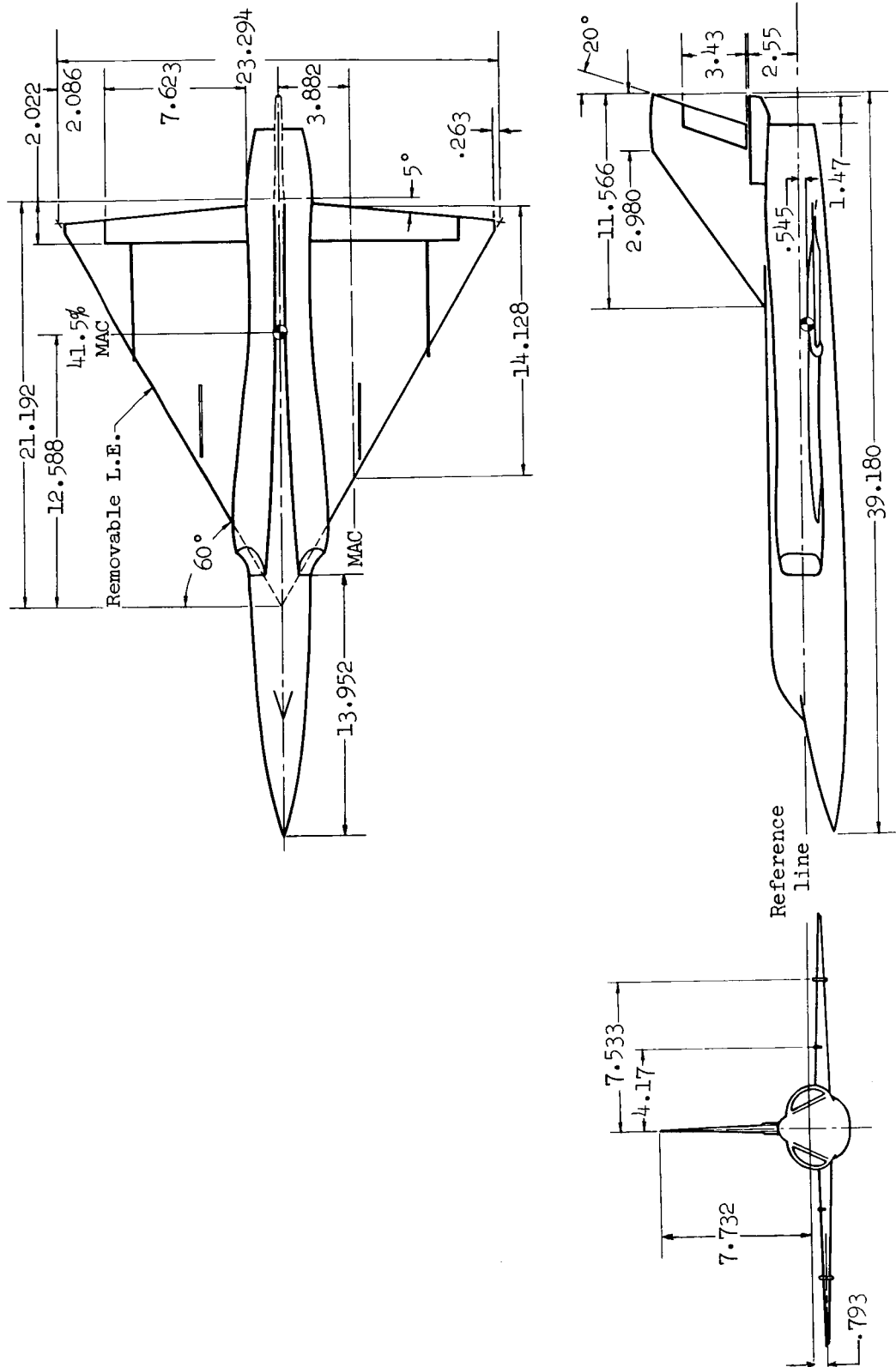
(b) Three-view drawing.

Figure 3.- Continued.
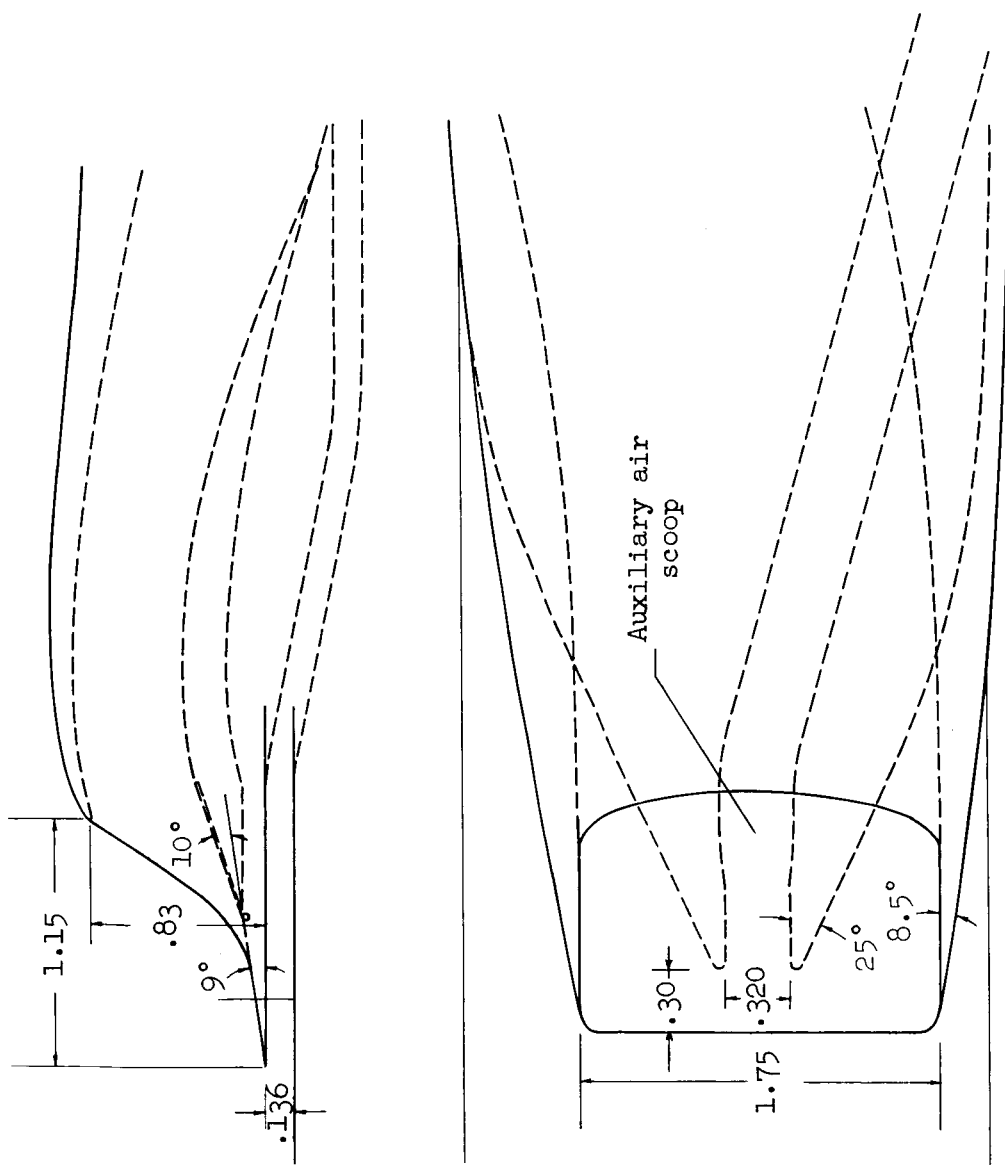
(c) Inlet details.

Figure 3.- Concluded.
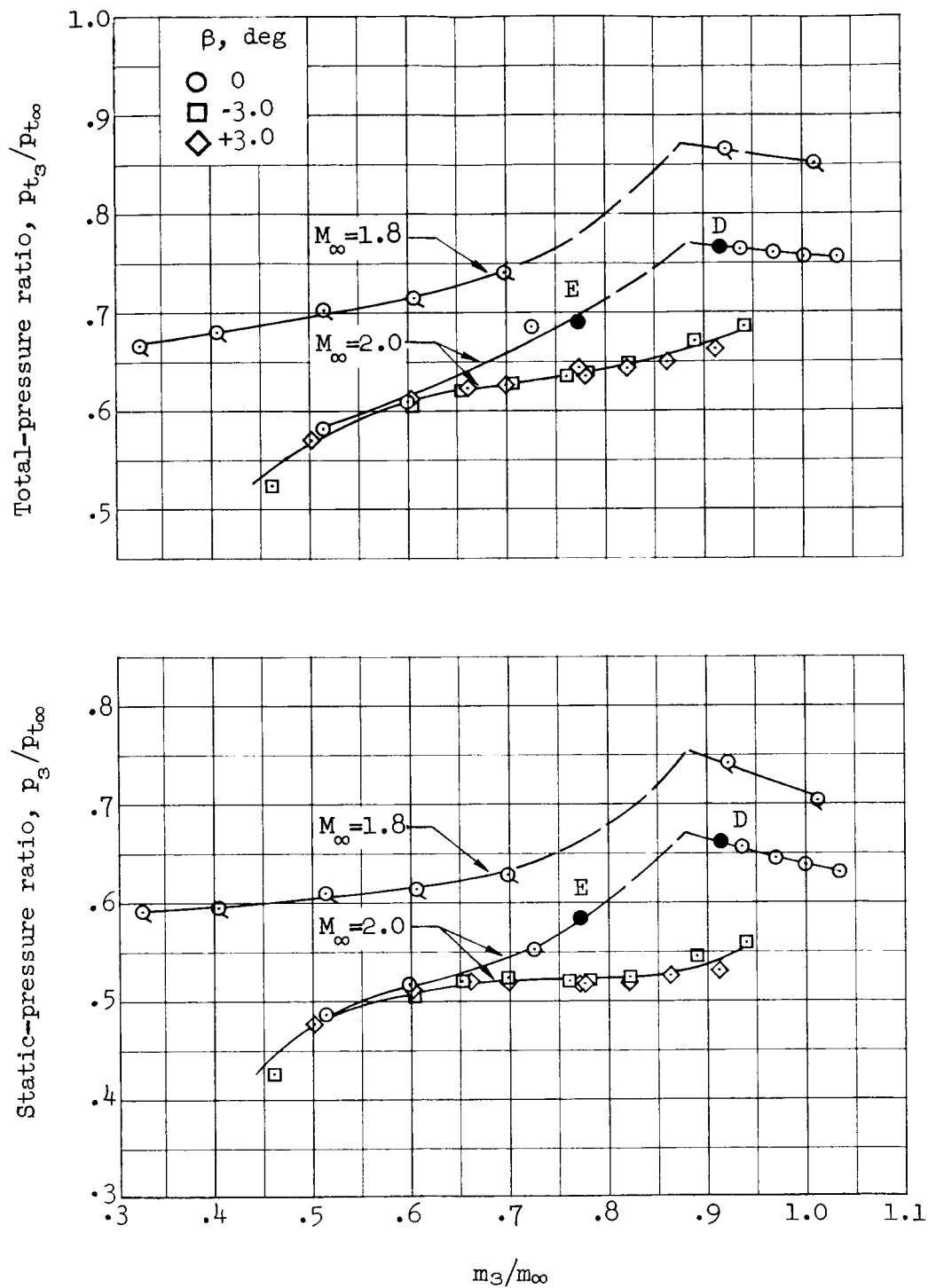
Figure 4.- Inlet system static- and total-pressure ratio characteristics; Model A, $\alpha = 1.0^\circ$.

Point D
$m_3/m_\infty = 0.914$

Point E
$m_3/m_\infty = 0.771$

Figure 5.- Schlieren photographs showing symmetric and asymmetric inlet flow; Model A, $M_\infty = 2.0$, $\alpha = 1.0°$, $\beta = 0°$.
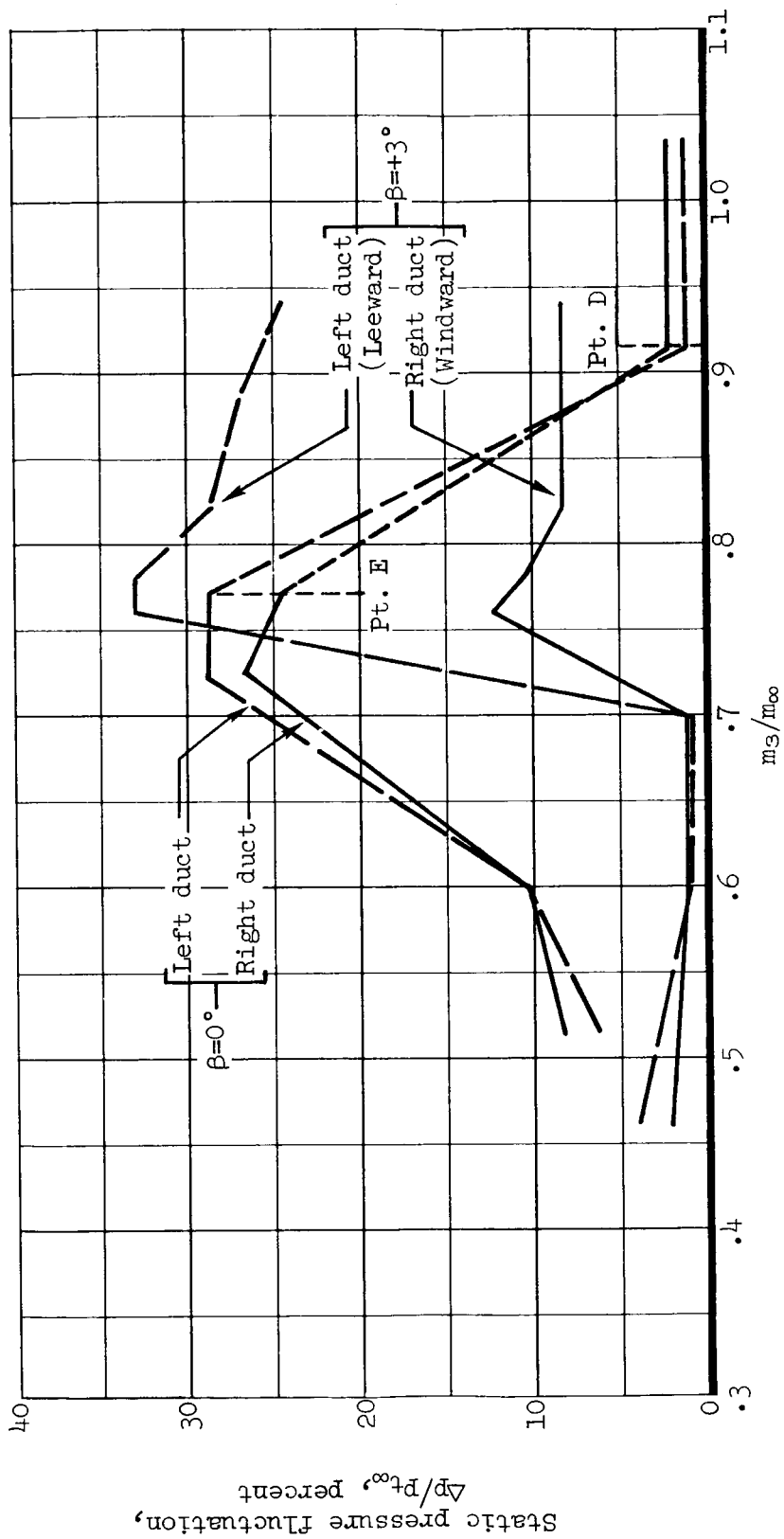
Figure 6.- Static-pressure unsteadiness characteristics; Model A, $M_\infty = 2.0$, $\alpha = 1.0°$.

O Supercritical

□ Subcritical
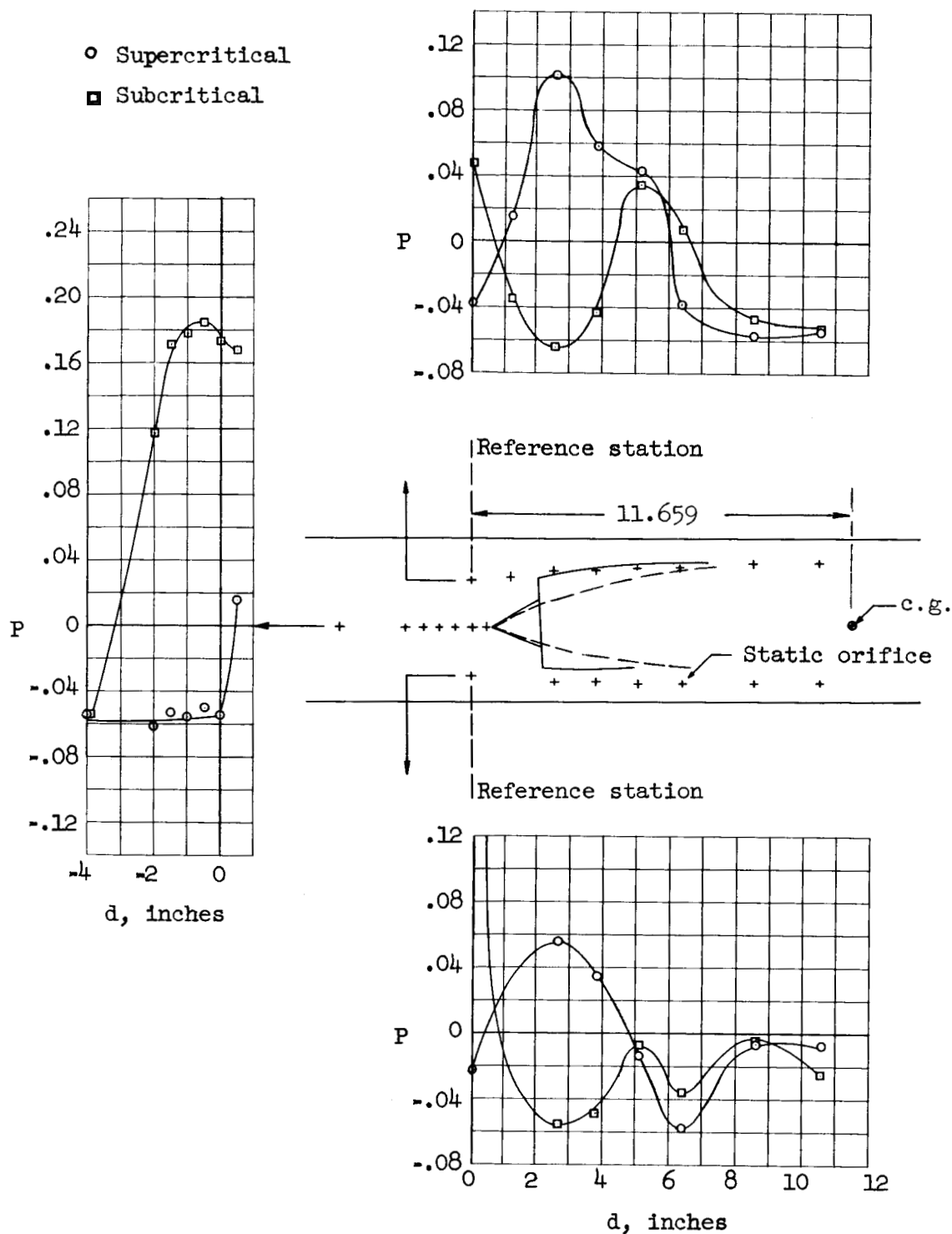
Figure 7.- Fuselage static-pressure distribution as affected by twin-duct
flow asymmetry; Model A, $M_\infty = 2.0$, $\alpha = 1.0^\circ$, $\beta = 0^\circ$.
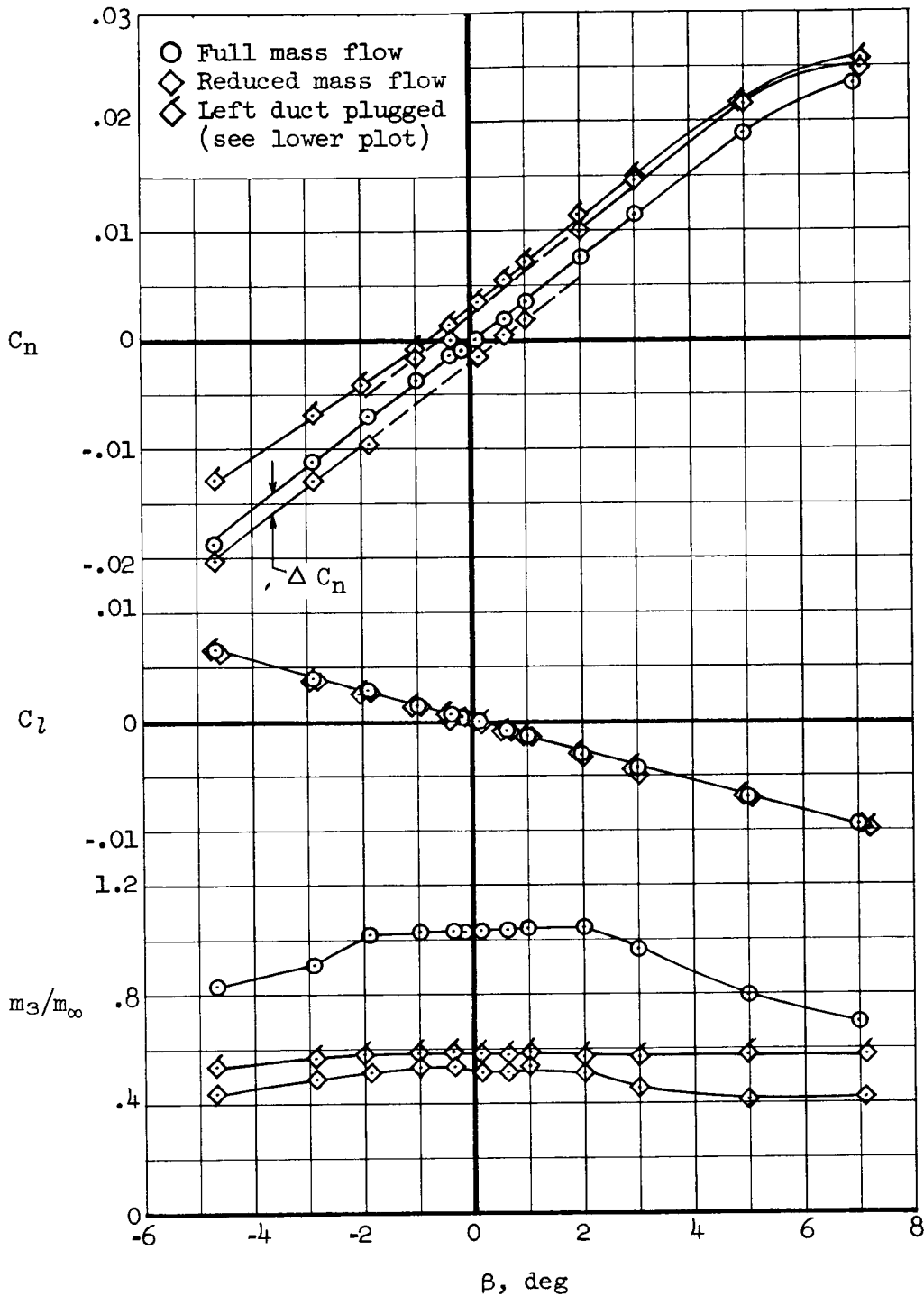
(a) $\alpha = 1.0^{\circ}$

Figure 8.- Lateral stability characteristics as affected by duct
mass-flow ratio; Model A, tail on, $M_{\infty} = 2.0$.
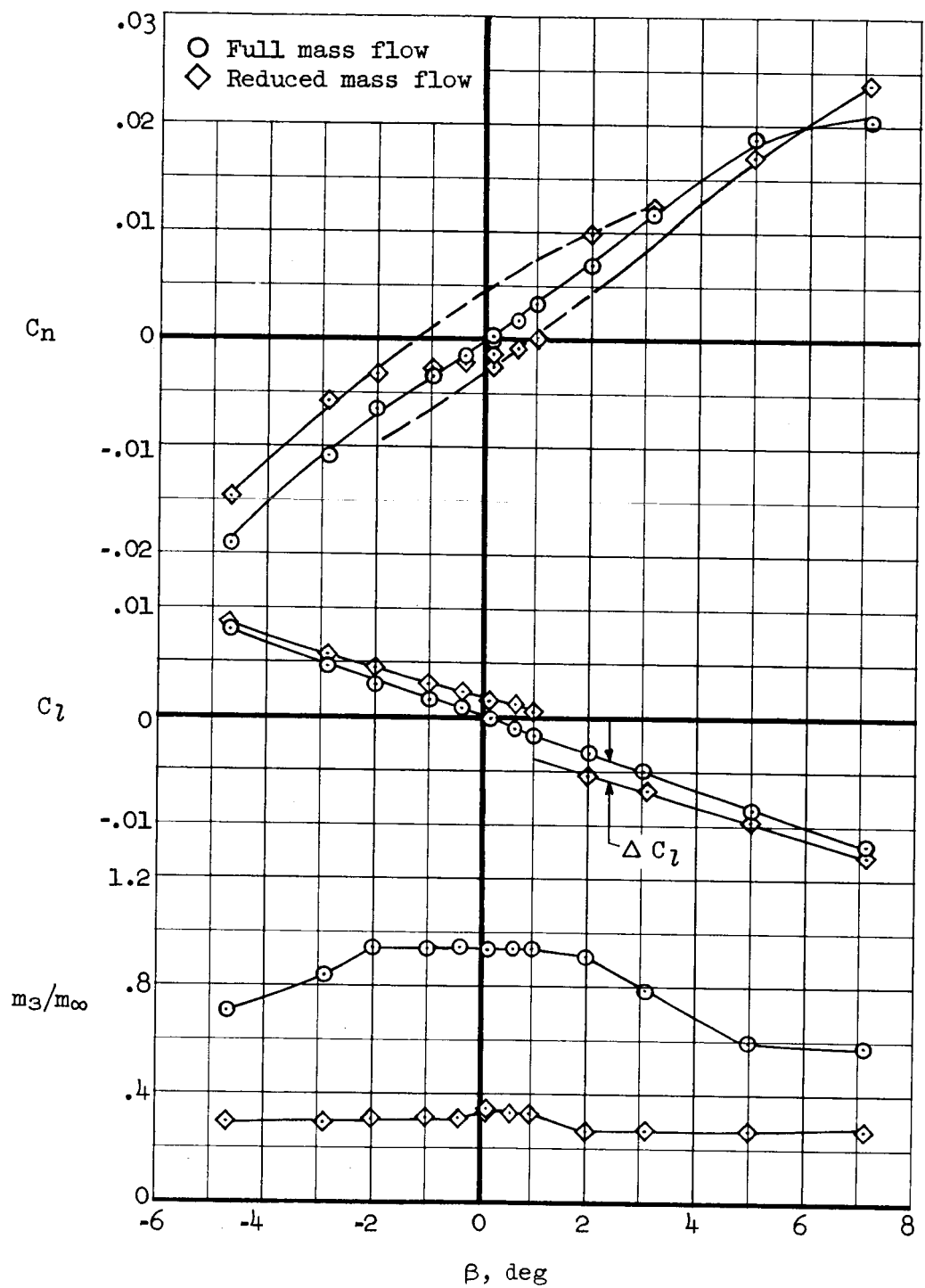
(b) $\alpha = 8.6°$

Figure 8.- Concluded.
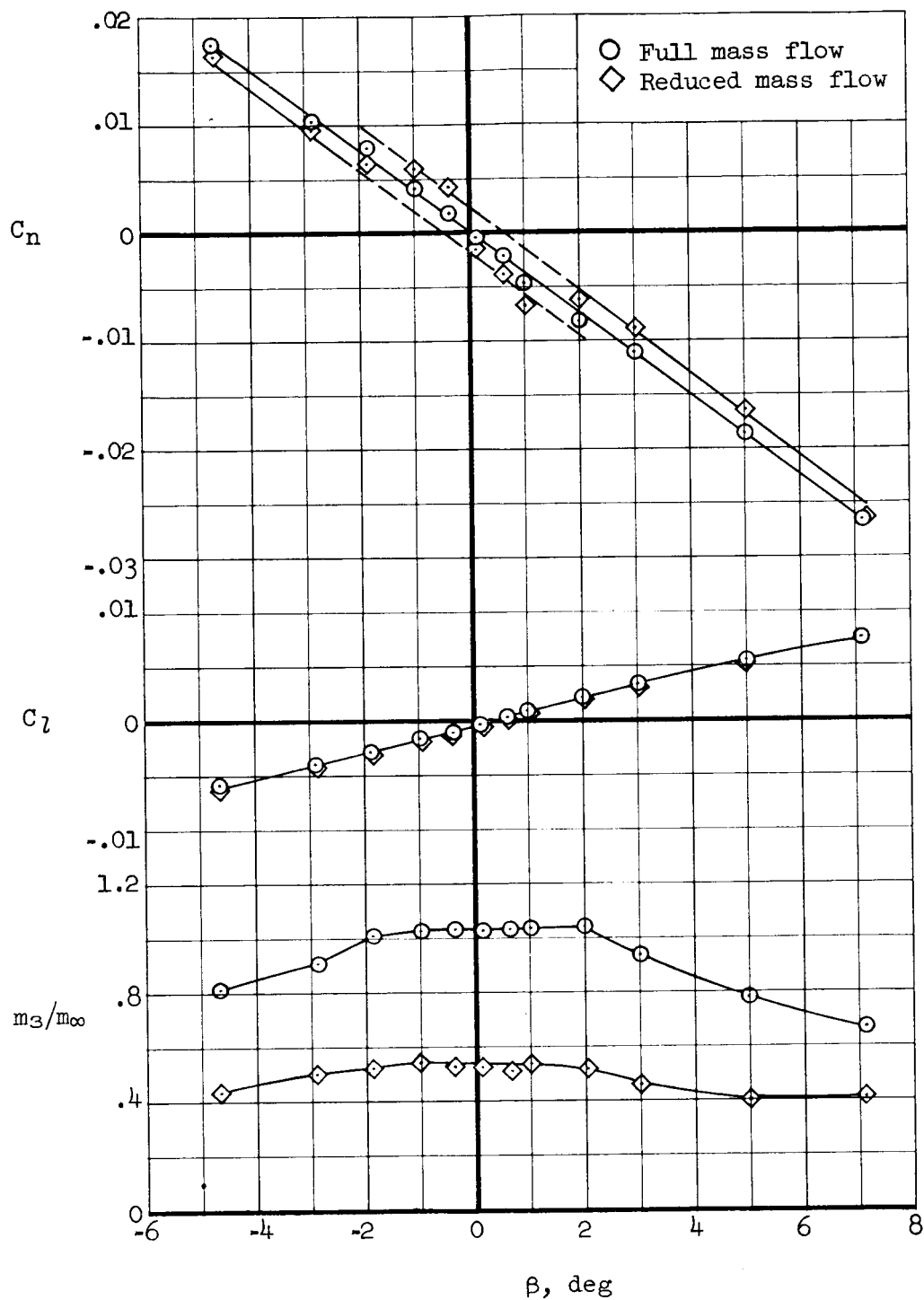
(a) $\alpha = 1.0^{\circ}$

Figure 9.- Lateral stability characteristics as affected by duct
mass-flow ratio; Model A, tail off, $M_{\infty} = 2.0$.

(b) $\alpha = 8.6^{o}$
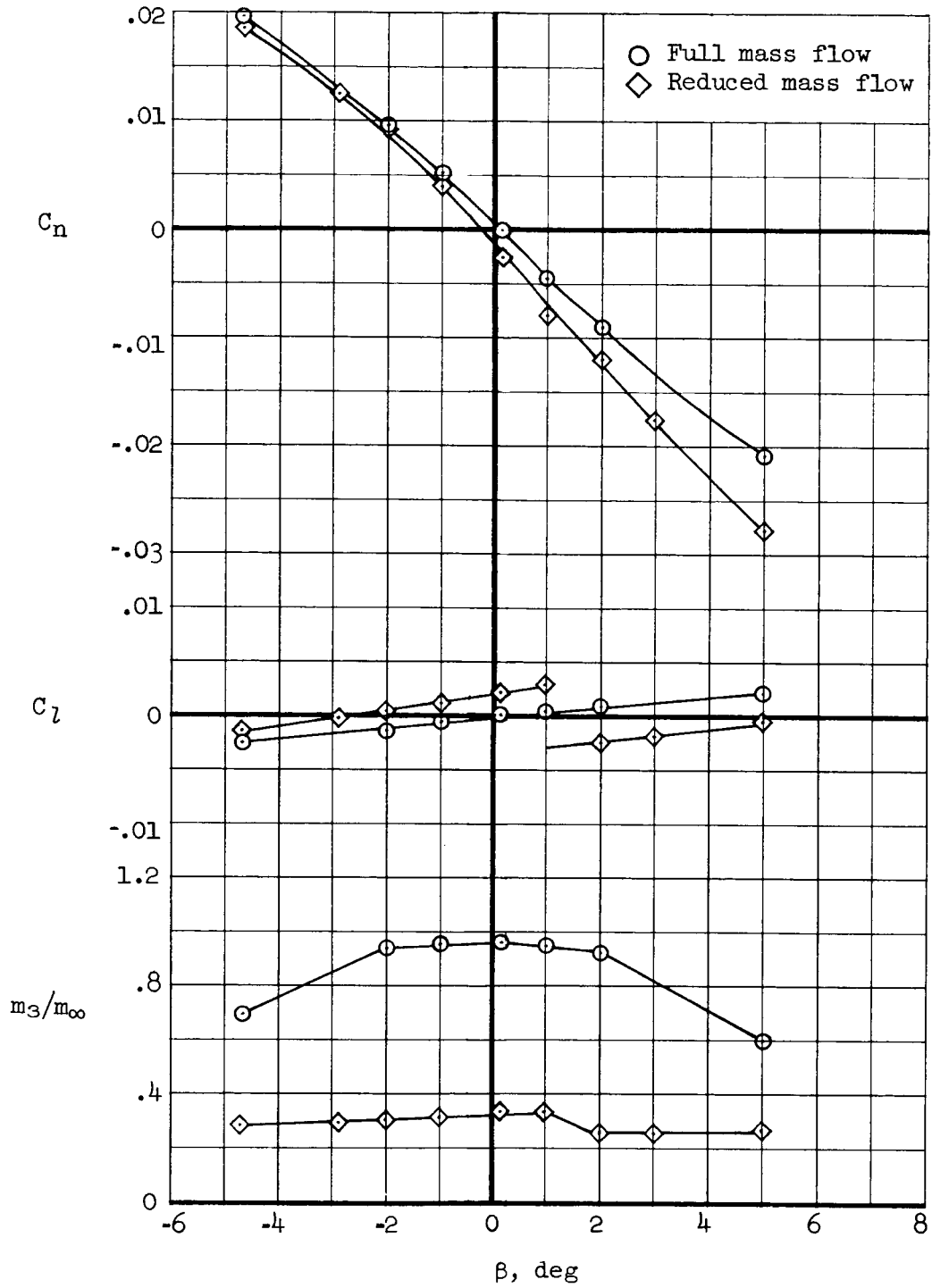
Figure 9.- Concluded.
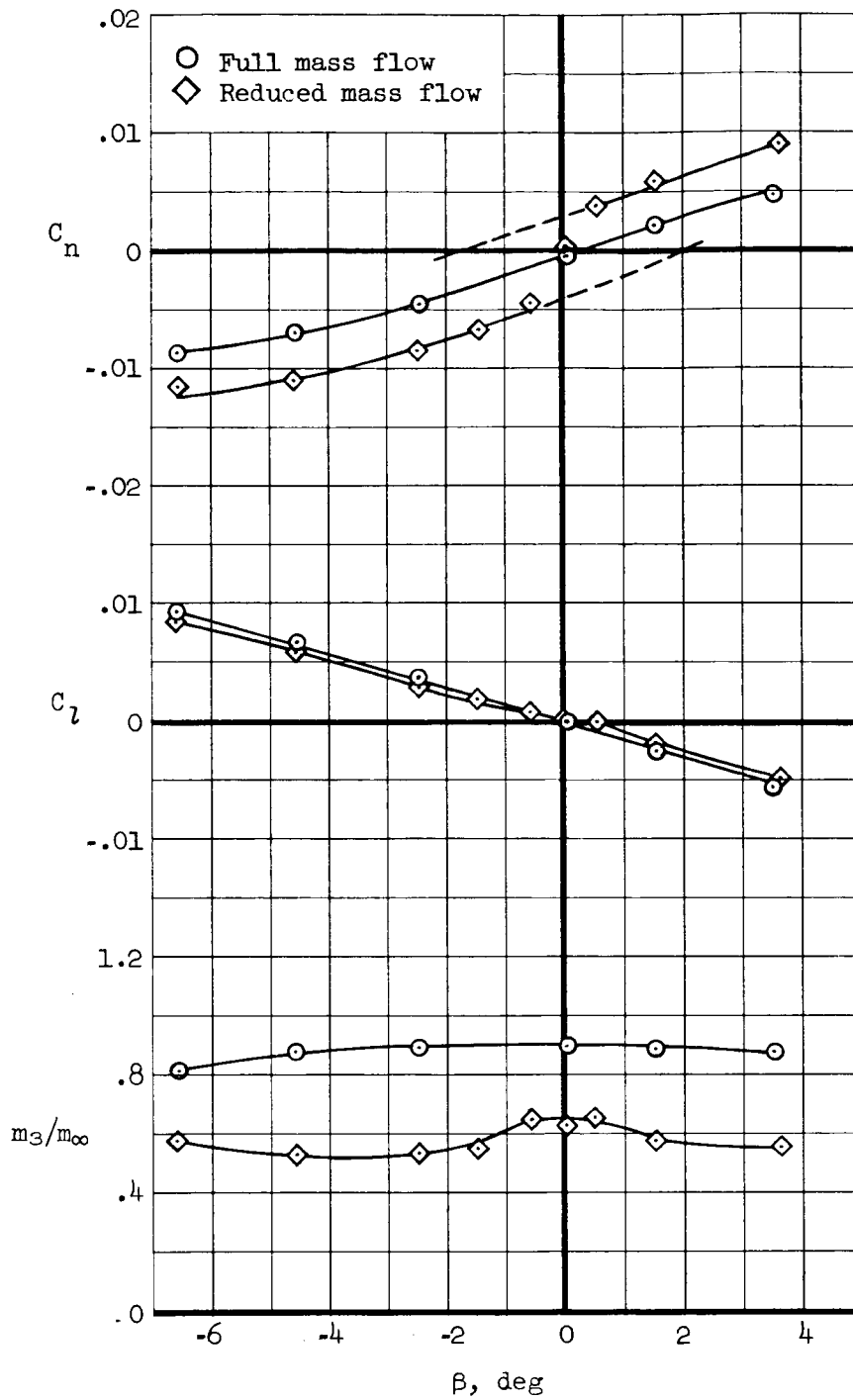
(a) $\alpha = 1.0^\circ$

Figure 10.- Lateral stability characteristics as affected by duct mass-flow ratio; Model B, tail on, $M_\infty = 2.20$.

(b) $\alpha = 7^{O}$
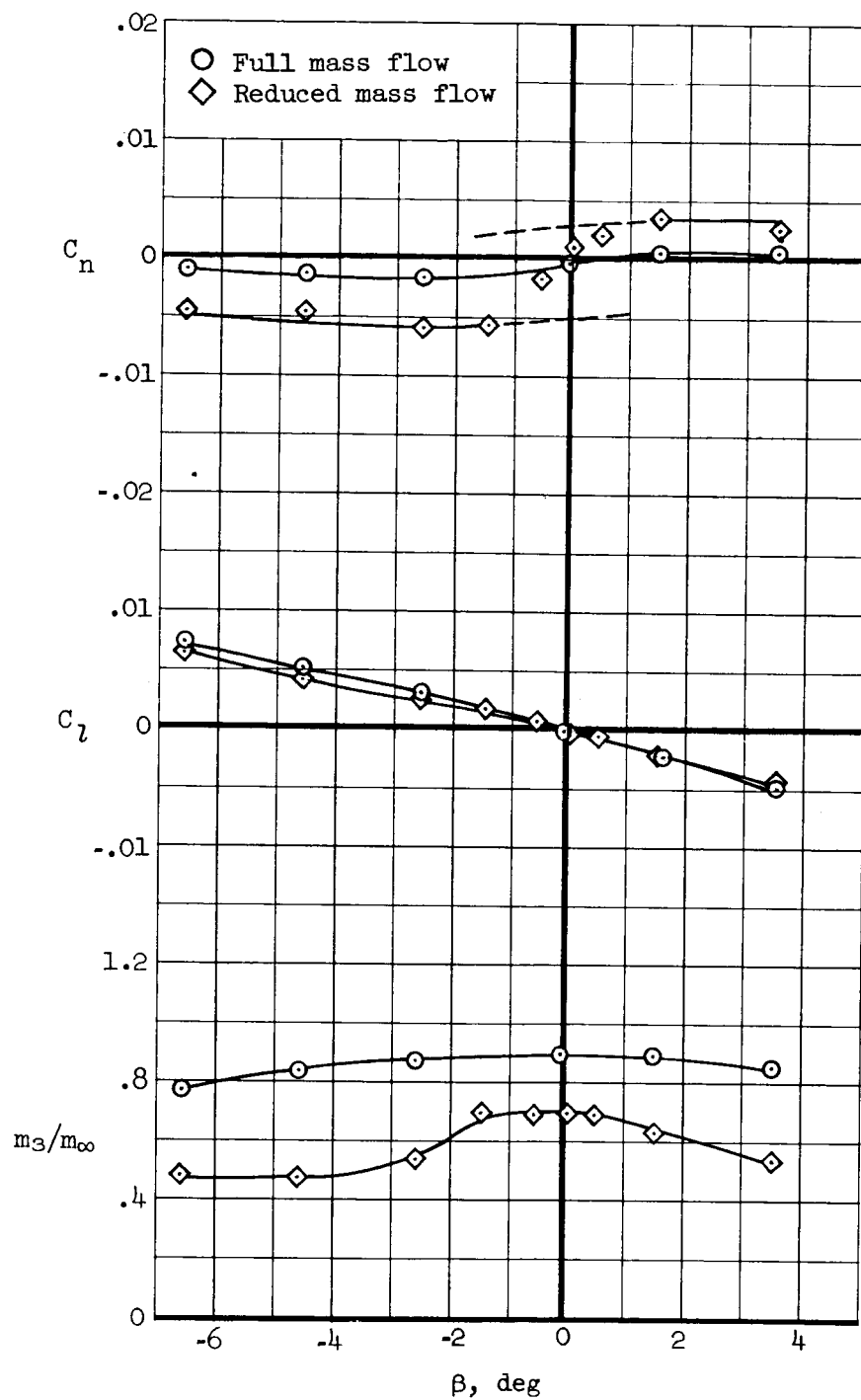
Figure 10.- Concluded.
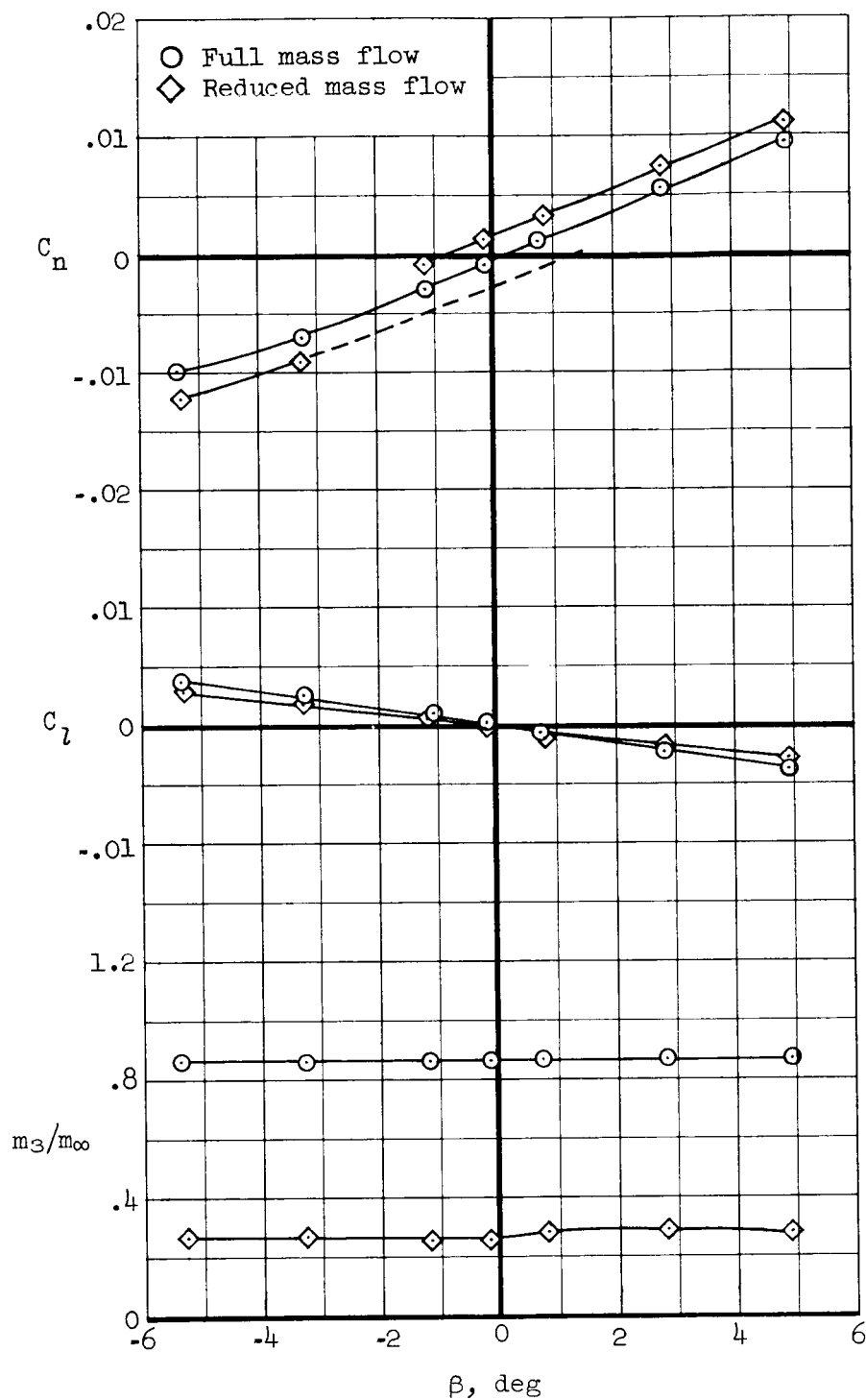
(a) $\alpha = 1.0^\circ$

Figure 11.- Lateral stability characteristics as affected by duct
mass-flow ratio; Model C, tail on, $M_\infty = 2.1$.
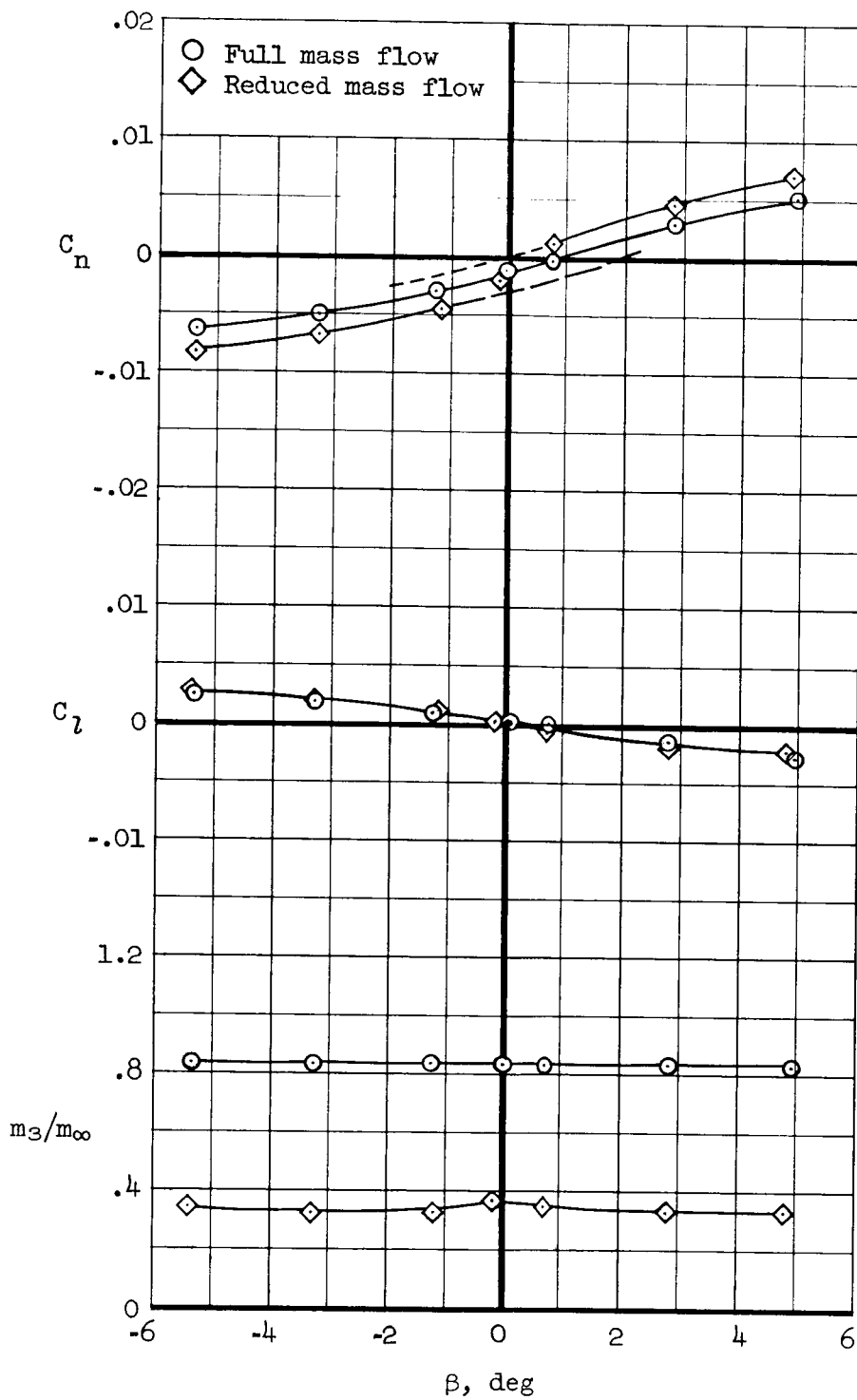
(b) $\alpha = 7.6^{\circ}$

Figure 11.- Concluded.
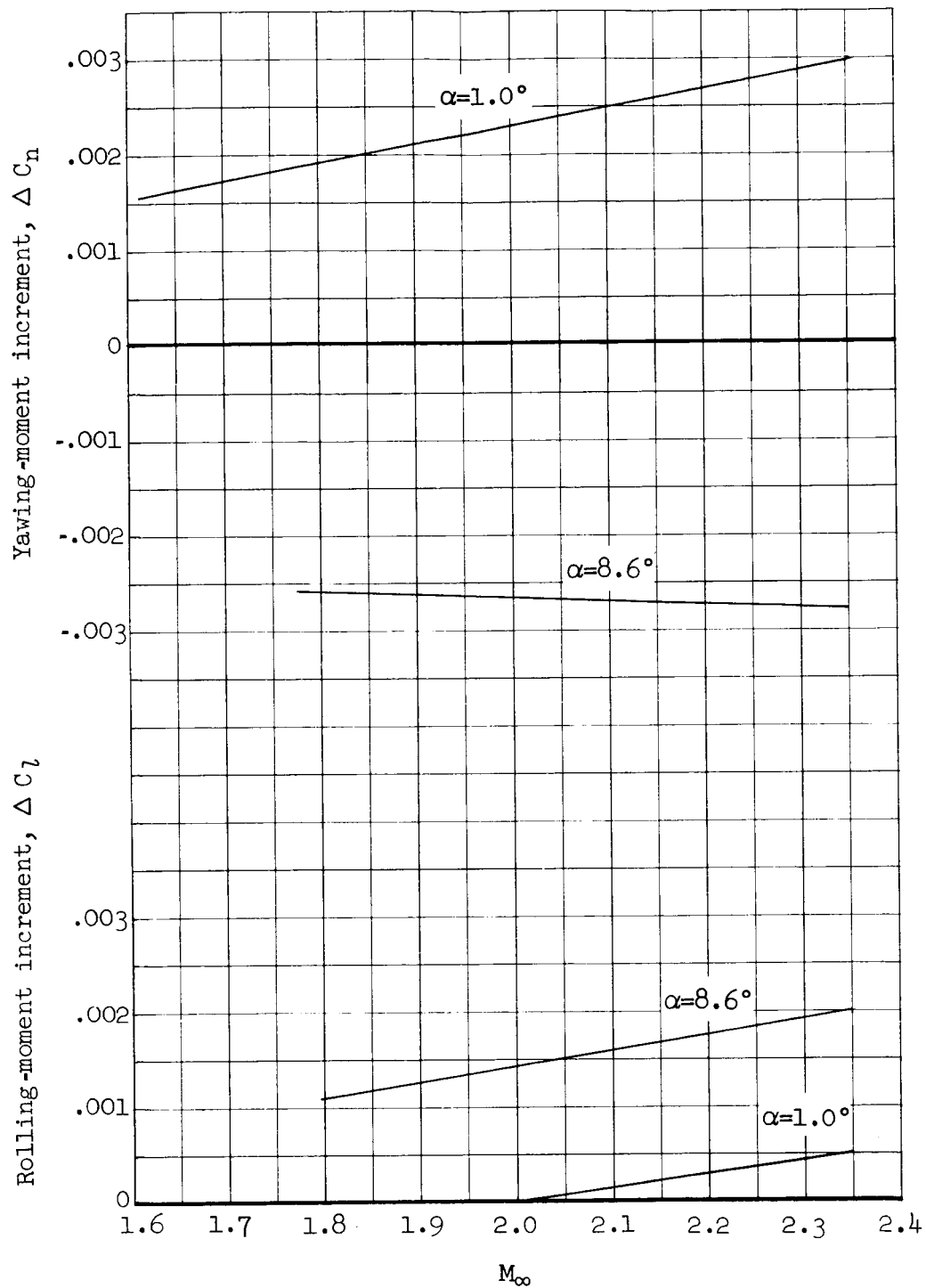
Figure 12.- Incremental variations in yawing-moment and rolling-moment coefficients for the range of test Mach numbers; Model A.
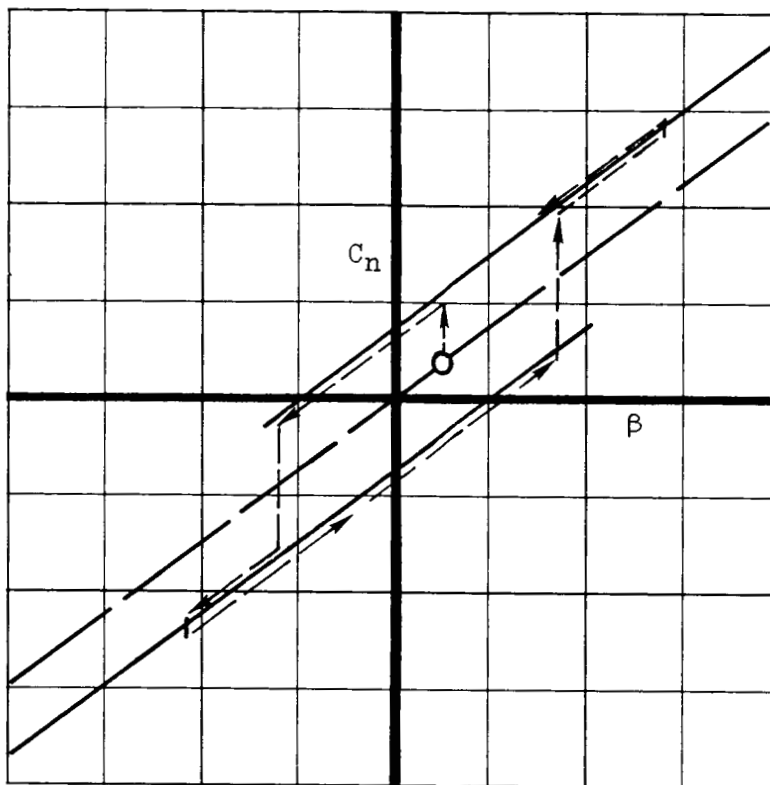
(a) Low angle of attack.
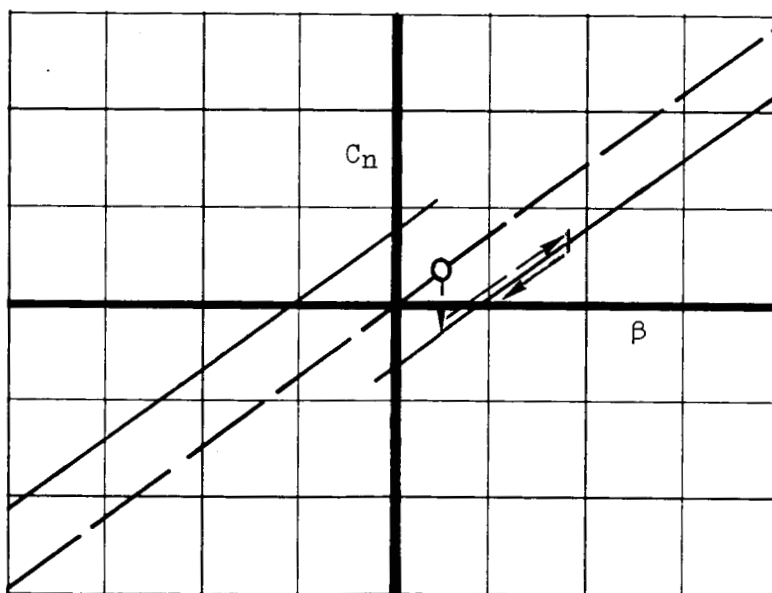
(b) High angle of attack.

Figure 13.- Aircraft yawing motions as a result of duct-flow asymmetry at reduced mass-flow ratios.
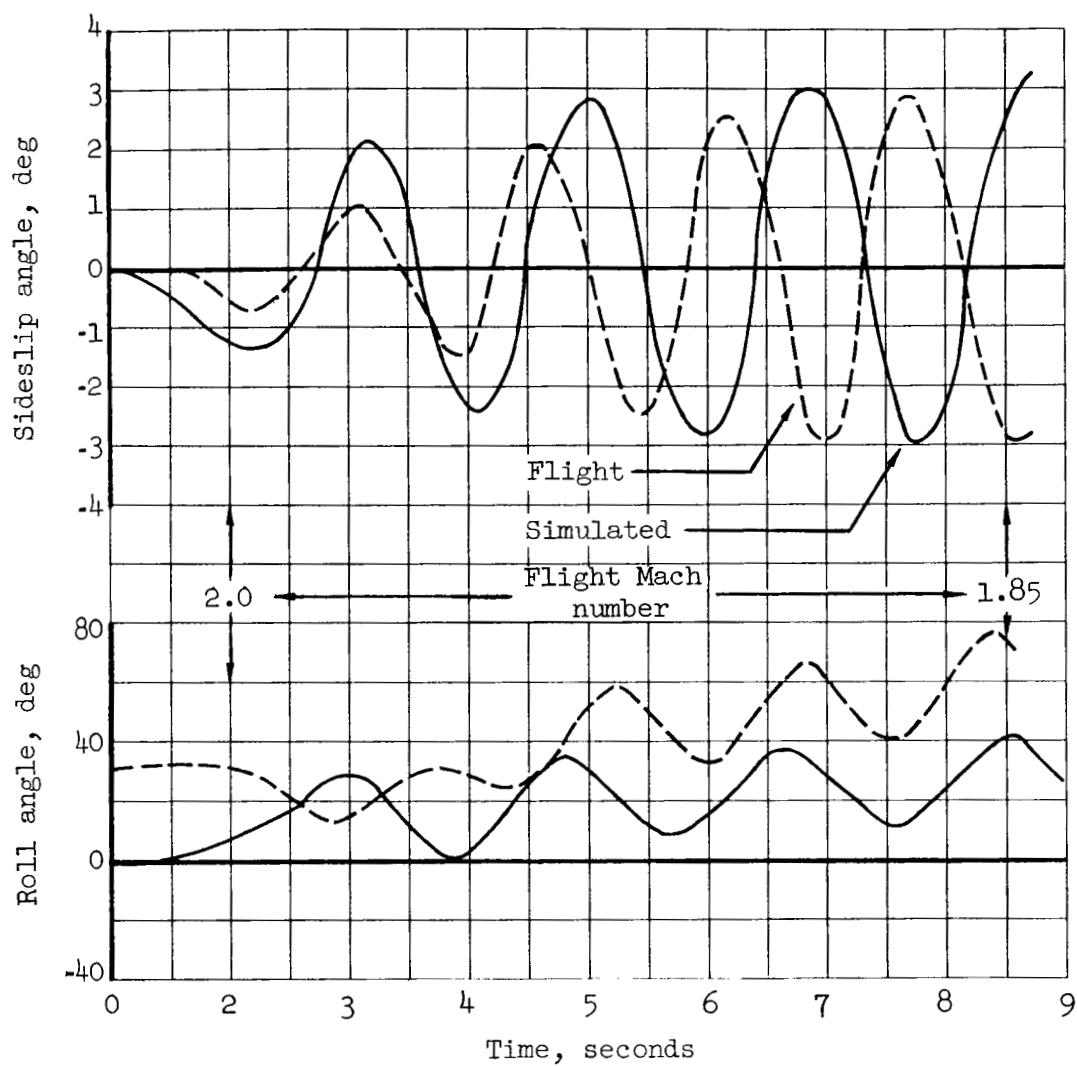
Figure 14.- Time-history comparison of aircraft motions as recorded in
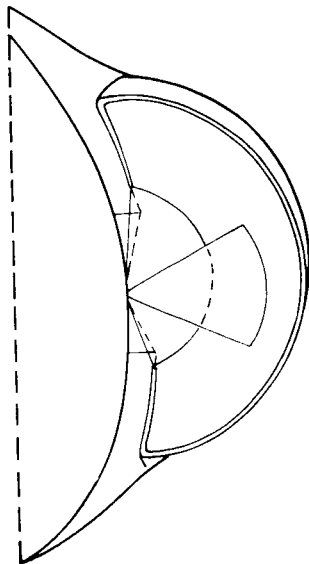flight and by flight simulation (ref. 8).
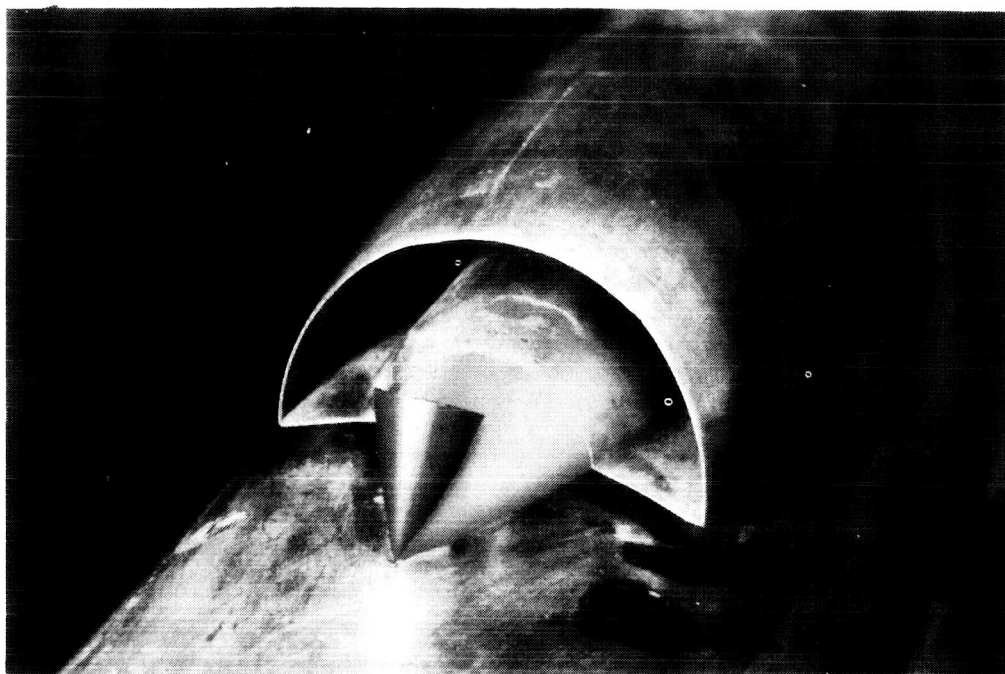
(a) Tilting cone deflector.

A-22624.1

(b) Cone plug deflector.

A-22625

Figure 15.- Photographs of flow deflectors used to reduce duct flow asymmetry; Model A.

.10

1.00

.032

65°

Section A-A

.37

1.40

.44R
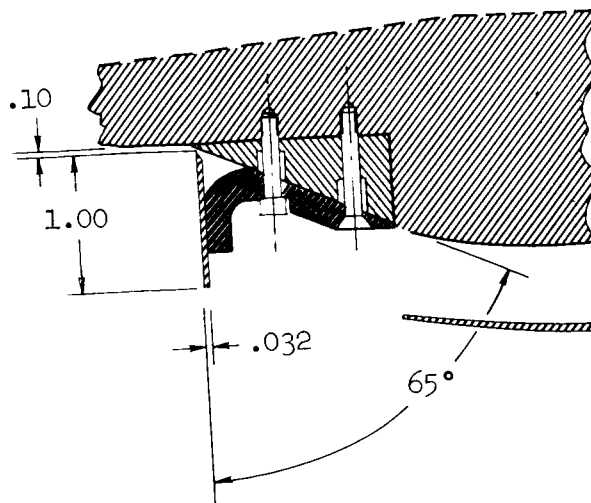
A

A
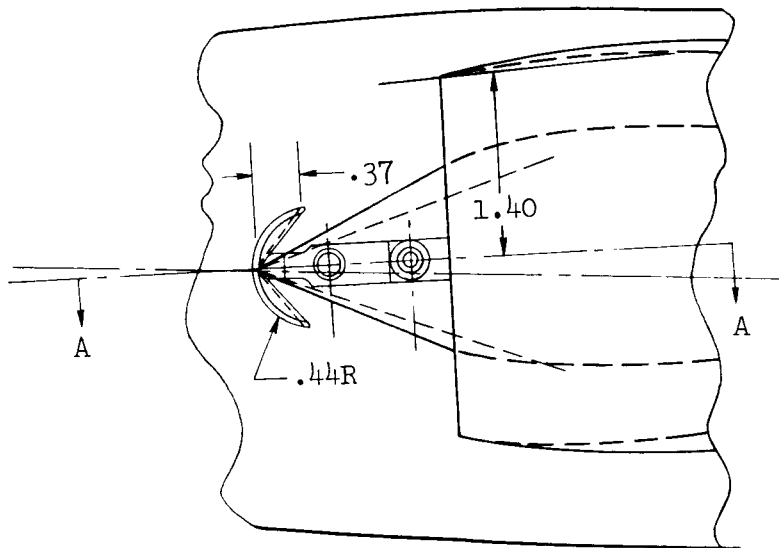
All dimensions in inches

Figure 16.- Detail sketch of tilting cone flow deflector; Model A.
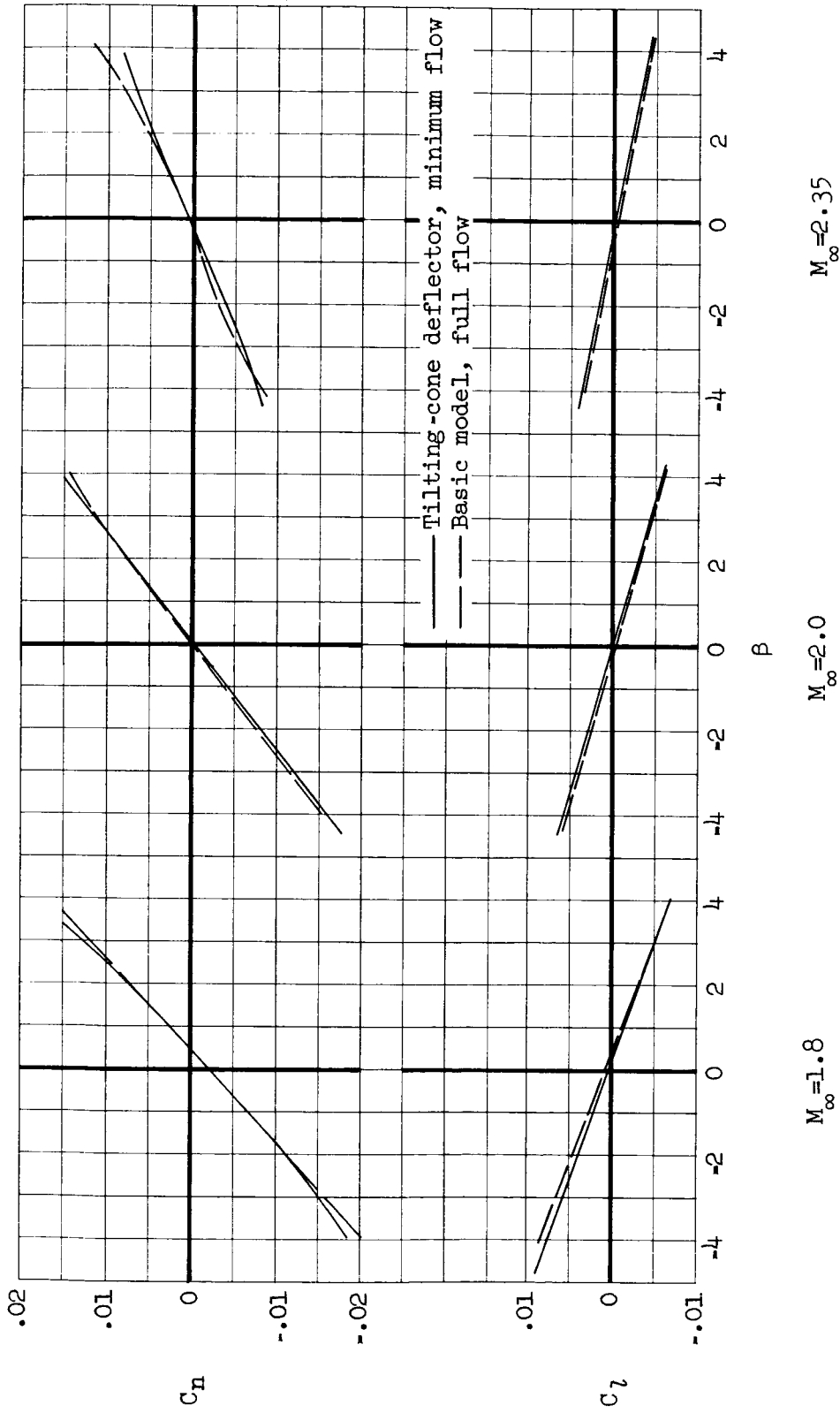
Figure 17.- Effect of flow deflectors on basic lateral stability for three test Mach numbers; Model A, α = 1.0°.

$m_3/m_\infty = 1.019$
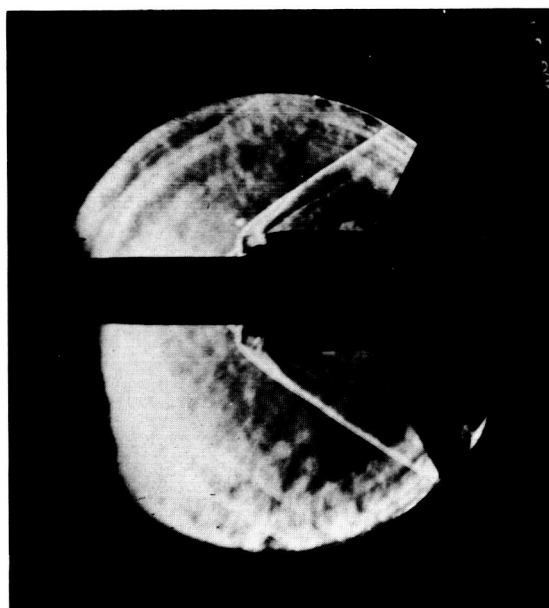$\beta = -2.0^o$

$m_3/m_\infty = 0.819$
$\beta = -2.0^o$

(a) Basic model.

$m_3/m_\infty = 0.366$
$\beta = 0^o$
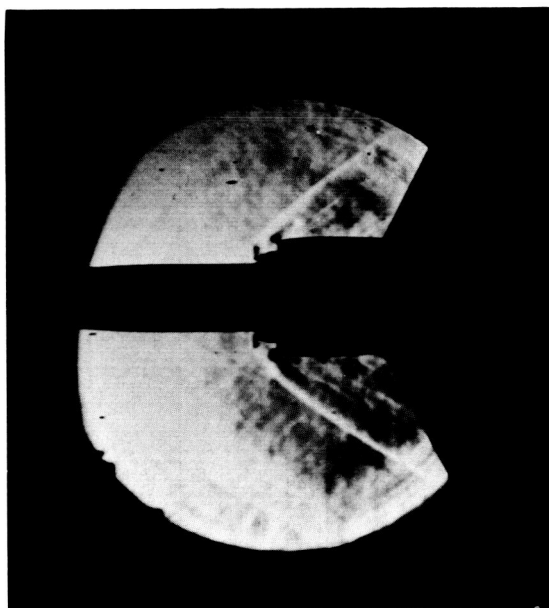
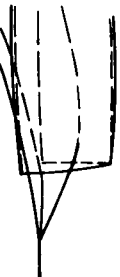$m_3/m_\infty = 0.218$
$\beta = -2.0^o$

(b) Basic model with deflectors.

Figure 18.- Schlieren photographs showing the effect of flow deflectors on inlet flow; Model A, $M_\infty = 2.0$, $\alpha = 1.0^o$.

NOTES: (1) Reynolds number is based on the diameter of a circle with the same area as that of the capture area of the inlet.

(2) The symbol * denotes the occurrence of buzz.

Report and facility	Description			Test parameters					Test data			Performance		Remarks
	Configuration	Number of oblique shocks	Type of boundary-layer control	Free-stream Mach number	Reynolds number × 10^{-6}	Angle of attack, deg	Angle of yaw, deg	Drag	Inlet-flow profile	Discharge-flow profile	Flow picture	Maximum total-pressure recovery	Mass-flow ratio	
NASA TM X-94 Ames 9- by 7-ft wind tunnel		1	Diverter formed by undercut-ting fuselage-mounted cone	2.0 1.8	2.0 2.2	1.0 1.0	0,+3,−3 0,+3,−3				✓	0.77 .87	1.04 1.01	No attempt made to optimize inlet performance.
NASA TM X-94 Ames 9- by 7-ft wind tunnel		1	Diverter formed by undercut-ting fuselage-mounted cone	2.0 1.8	2.0 2.2	1.0 1.0	0,+3,−3 0,+3,−3				✓	0.77 .87	1.04 1.01	No attempt made to optimize inlet performance.
NASA TM X-94 Ames 9- by 7-ft wind tunnel		1	Diverter formed by undercut-ting fuselage-mounted cone	2.0 1.8	2.0 2.2	1.0 1.0	0,+3,−3 0,+3,−3				✓	0.77 .87	1.04 1.01	No attempt made to optimize inlet performance.
NASA TM X-94 Ames 9- by 7-ft wind tunnel		1	Diverter formed by undercut-ting fuselage-mounted cone	2.0 1.8	2.0 2.2	1.0 1.0	0,+3,−3 0,+3,−3				✓	0.77 .87	1.04 1.01	No attempt made to optimize inlet performance.

Bibliography

These strips are provided for the convenience of the reader and can be removed from this report to compile a bibliography of NACA inlet reports. This page is being added only to inlet reports and is on a trial basis.

CONFIDENTIAL